Quadrupole moments and proton-neutron structure in p-shell mirror nuclei

Mark A. Caprio and Patrick J. Fasano
Department of Physics, University of Notre Dame, Notre Dame, Indiana 46556-5670, USA

Pieter Maris
Department of Physics and Astronomy, Iowa State University, Ames, Iowa 50011-3160, USA

Anna E. McCoy
Institute for Nuclear Theory, University of Washington, Seattle, Washington 98195-1550, USA
(Dated: September 21, 2021)

Electric quadrupole ($E2$) matrix elements provide a measure of nuclear deformation and related collective structure. Ground-state quadrupole moments in particular are known to high precision in many p-shell nuclei. While the experimental electric quadrupole moment only measures the proton distribution, both proton and neutron quadrupole moments are needed to probe proton-neutron asymmetry in the nuclear deformation. We seek insight into the relation between these moments through the *ab initio* no-core configuration interaction (NCCI), or no-core shell model (NCSM), approach. Converged *ab initio* calculations for quadrupole moments are particularly challenging, due to sensitivity to long-range behavior of the wave functions. We therefore study more robustly-converged *ratios* of quadrupole moments: across mirror nuclides, or of proton and neutron quadrupole moments within the same nuclide. In calculations for mirror pairs in the p shell, we explore how well the predictions for mirror quadrupole moments agree with experiment and how well isospin (mirror) symmetry holds for quadrupole moments across a mirror pair. The comparison with experiment confirms the predictive power of the *ab initio* description, indicating that the predicted ratios are physically relevant for understanding proton-neutron structure as well.

arXiv:2106.12128v3 [nucl-th] 18 Sep 2021

I. INTRODUCTION

Electric quadrupole ($E2$) matrix elements, including quadrupole moments, provide a principal measure of nuclear deformation, rotation, and related collective structure [1–5]. To probe the proton-neutron asymmetric aspects of the nuclear deformation, both proton and neutron quadrupole observables are needed. For instance, in an axially symmetric rotational nucleus [4], the ratio of proton and neutron quadrupole moments indicates the relative contributions of protons and neutrons to the overall deformation, that is, the ratio of quadrupole moments in the rotational intrinsic frame. Alternatively, in a spherical shell-model description, an anomalously large quadrupole moment for one of the nucleonic species can be interpreted as an indicator of halo structure [6, 7].

While the ground state electric quadrupole moment is readily accessible via electromagnetic measurements [8], this observable provides access only to the quadrupole moment of the proton density distribution within the nucleus. Neutron quadrupole observables are at best indirectly measurable, *e.g.*, through nuclear inelastic hadron or α scattering [9]. For the neutron quadrupole moment, in particular, if we consider two nuclei forming a mirror pair, the approximate isospin symmetry of the nuclear system [10] implies that the behavior of the protons in one member of the pair provides a proxy for the behavior of the neutrons in the other, and *vice versa*. Thus, by mirror symmetry, we can deduce the neutron quadrupole moment of one nucleus from the measured proton quadrupole moment of the other. However, this approach is limited to cases in which the quadrupole moments are experimentally accessible for both members of the mirror pair. Moreover, it relies on the assumption, possibly imperfect, of mirror symmetry.

We therefore seek further insight from *ab initio* theory into the proton and neutron quadrupole moments, and their relation, in light (p-shell) nuclei. *Ab initio* approaches to the nuclear many-body problem do not impose any specific *a priori* model assumptions, yet they are found to reproduce signatures of phenomena involving quadrupole deformation, clustering [11–16], and rotation [17–22].

Before extracting physical information from *ab initio* calculations, we must first identify the extent to which convergence is obtained for the relevant observables. In practice, the many-body Hilbert space used in an *ab initio* calculation must be truncated to finite size. Calculations in progressively larger spaces, involving progressively less severe truncations, provide results which converge towards those which would be obtained by solving the full, untruncated many-body problem. Nonetheless, the accuracy of calculated observables is limited by computational constraints on the spaces which can be accommodated.

The degree of convergence varies tremendously depending upon the observable under consideration. It is particularly challenging to obtain meaningful *ab initio* calculations for $E2$ matrix elements, including quadrupole moments, due to their sensitivity to the large-distance behavior (or tails) of the wave functions. While the no-core configuration interaction (NCCI) [23], or no-core shell model (NCSM), approach has considerable success in providing calculations for, *e.g.*, energies and mag-

netic dipole observables, throughout the p shell [24], even order-of-magnitude calculations for $E2$ matrix elements are elusive.

To circumvent this limitation, we recognize that *ratios* of $E2$ matrix elements can be more robustly calculated than individual matrix elements. If the matrix elements entering into the ratio involve structurally similar states, so that convergence properties are similar, errors from truncation of the many-body space can cancel in the ratio. Such behavior has already been noted for $E2$ matrix elements among states within the same rotational band [18, 22], or between rotational bands with related structures [25], and for the $E2$ strengths of mirror transitions [26]. Prior calculations of the ratio of proton and neutron quadrupole moments [18] have suggested that this ratio may be similarly robust, at least in a limited sampling of rotational states (see Fig. 18 of Ref. [18]).

In the present work, to investigate proton-neutron asymmetry in quadrupole structure, we consider NCCI calculations for two ratios: (1) that of the proton (or electric) quadrupole moments for the ground states of both members of a mirror pair, as accessible in experiment, and (2) that of the proton and neutron quadrupole moments within the ground state of a single nuclide, which provides the more direct structural measure. To the extent that convergence is obtained for these ratios, and to the extent that the results are found to be robust with respect to the choice of internucleon interaction, we wish to understand the following:

(1) How well do the predictions agree with experiment, in mirror pairs for which the quadrupole moments of both members are experimentally known [8]?

(2) To what extent does mirror symmetry actually hold for the proton and neutron quadrupole moments across a mirror pair, so that the mirror ratio may indeed be taken as equivalent to the ratio of proton and neutron quadrupole moments within a single member of the pair?

We carry out NCCI calculations of ground-state quadrupole moments for a comprehensive set of pairs of mirror nuclei in the p shell. Namely, we consider all mirror pairs in which both members are particle-bound (as well as one involving an extremely narrow ground-state resonance) and in which the angular momentum selection rule permits a nonzero quadrupole moment. We compare results based on the Daejeon16 interaction [27], JISP16 interaction [28], and LENPIC interaction taken to N^{2}LO in chiral effective field theory (EFT) [29, 30].

In the following, after a brief overview of the mirror pairs being considered and the available experimental data (Sec. II), we examine the convergence properties of the ground-state quadrupole moments, and their ratios, obtained in the NCCI calculations for these nuclei (Sec. III). We then examine the accuracy with which mirror symmetry holds for the calculated ratios, given the isospin symmetry breaking provided by the interactions considered here (Sec. IV). Approaches to interpreting the calculated ratio of neutron and quadrupole moments as an indicator of proton-neutron nuclear structure, in terms of cluster [31] or SU(3) [32, 33] descriptions, are suggested (Sec. V).

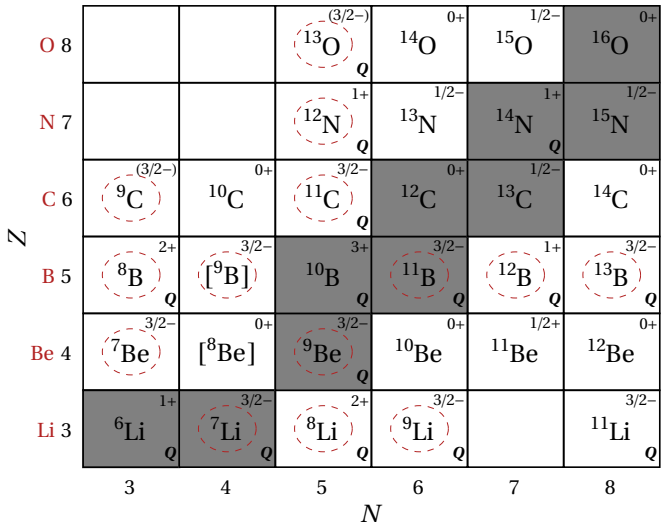

FIG. 1. Overview of particle-bound nuclides in the p shell, indicating ground-state angular momentum and parity [34–38]. Brackets indicate a particle-unbound but narrow ($\lesssim 1$ keV) ground-state resonance. Nuclides with measured ground-state quadrupole moments [8] are indicated with the letter "Q". Those cases in which both members of a mirror pair are particle-bound and have ground-state angular momenta supporting a quadrupole moment, the criterion for inclusion in the present calculations, are highlighted (dashed circles). Shading indicates stable isotopes.

II. MIRROR QUADRUPOLE MOMENTS IN THE p SHELL

We focus on mirror pairs in the p shell for which both members are particle-bound. The full set of bound p-shell nuclei [34–38] is summarized in Fig. 1, along with ground-state angular momentum and parity assignments. For present purposes, we also include exceptionally narrow ground-states resonances, indicated by brackets in Fig. 1. (In particular, although ^{9}B is unstable to proton emission, its ground state has a width of only ~ 0.5 keV [35].)

Since the quadrupole moment vanishes identically for any state with angular momentum $J < 1$, mirror pairs with ground state $J = 0$ (and thus all even-even nuclei) or 1/2 are excluded. This leaves us with the following mirror pairs for consideration (circled in Fig. 1): $A = 7$ (^{7}Li/^{7}Be), 8 (^{8}Li/^{8}B), 9 (^{9}Be/^{9}B), 9′ (^{9}Li/^{9}C), 11 (^{11}B/^{11}C), 12 (^{12}B/^{12}N), and 13′ (^{13}B/^{13}O). Here, for odd A, we indicate non-nearest neighbor mirror pairs, namely with $T_z = \pm 3/2$, by placing a prime on the value of A, while the rest have $T_z = \pm 1/2$. The odd-odd mirror pairs all have the minimal $T_z = \pm 1$.

Ground-state electric quadrupole moments are experimentally known (as indicated by a "Q" in Fig. 1) for most

TABLE I. Experimental ground-state quadrupole moments [8] for the p-shell mirror pairs considered here, and prior *ab initio* GFMC predictions [39] (discussed in Sec. III). Ratios within a mirror pair are deduced where possible, and the uncertainty on the ratio is obtained assuming the uncertainties on the individual moments are uncorrelated.

Nuclide				Experiment		GFMC (AV18+IL7)	
A		(Z,N)	J^P	Q (fm^2)	Ratio	Q (fm^2)	Ratio
7	^{7}Li	$(3,4)$	$3/2^-$	$-4.00(3)$		$-4.0(1)$	
	^{7}Be	$(4,3)$	$3/2^-$	—	—	$-6.7(1)$[a]	$+1.68(5)$
8	^{8}Li	$(3,5)$	2^+	$+3.14(2)$		$+3.3(1)$	
	^{8}B	$(5,3)$	2^+	$+6.34(14)$	$+2.02(5)$	$+5.9(4)$	$+1.79(13)$
9	^{9}Be	$(4,5)$	$3/2^-$	$+5.29(4)$		$+5.1(1)$	
	^{9}B	$(5,4)$	$3/2^-$	—	—	$+4.0(3)$[a]	$+0.78(6)$
9′	^{9}Li	$(3,6)$	$3/2^-$	$-3.04(2)$		$-2.3(1)$	
	^{9}C	$(6,3)$	$(3/2^-)$	—	—	$-4.1(4)$	$+1.8(2)$
11	^{11}B	$(5,6)$	$3/2^-$	$+4.059(10)$			
	^{11}C	$(6,5)$	$3/2^-$	$\pm3.33(2)$	$\pm0.820(5)$		
12	^{12}B	$(5,7)$	1^+	$\pm1.32(3)$			
	^{12}N	$(7,5)$	1^+	$+1.00(9)$[b]	$\pm0.76(7)$		
13′	^{13}B	$(5,8)$	$3/2^-$	$(+)3.65(8)$			
	^{13}O	$(8,5)$	$3/2^-$	$\pm1.11(8)$	$\pm0.30(2)$		

[a] The GFMC quadrupole moments for ^{7}Be and ^{9}B provided in Table II of Ref. [39] are derived under proton-neutron interchange from wave functions for the mirror nuclides ^{7}Li and ^{9}Be (*i.e.*, from Q_n, assuming mirror symmetry). Furthermore, from entries marked with an asterisk in Table II of Ref. [39], indicating quadrupole moments derived under proton-neutron interchange from the wave function for the mirror nuclide, we may read off the calculated neutron quadrupole moments $Q_n(^8\mathrm{Li}) = +6.5(2)\,\mathrm{fm}^2$, $Q_n(^8\mathrm{B}) = +3.0(4)\,\mathrm{fm}^2$, $Q_n(^9\mathrm{Li}) = -3.7(1)\,\mathrm{fm}^2$, and $Q_n(^9\mathrm{C}) = -2.7(2)\,\mathrm{fm}^2$.

[b] The quadrupole moment for ^{12}N is tabulated in the Stone 2016 evaluation [8] as $+10.0(9)\,\mathrm{fm}^2$, or $+0.100(9)\,\mathrm{b}$ in the units adopted in that tabulation. The underlying experimental β-NMR results are those of Minamisono *et al.* [40], which permit the ^{12}N quadrupole moment to be deduced relative to that of the ^{14}N reference standard. As originally taken in conjunction with the ^{14}N quadrupole moment of Schirmacher *et al.* [41], the experimental results yielded a ^{12}N quadrupole moment of $+0.98(9)\,\mathrm{fm}^2$ [40], as also subsequently quoted in the Stone 2005 [42] and Kelley *et al.* 2012 [38] evaluations. However, the Stone 2016 evaluation [8] adopts an updated ^{14}N reference quadrupole moment from Pyykkö [43], which provides a 2% adjustment relative to the prior value. This yields a revised ^{12}N quadrupole moment of $+1.00(9)\,\mathrm{fm}^2$, or $+0.0100(9)\,\mathrm{b}$, as we take here. However, the value tabulated in Ref. [8] differs by a shifted decimal point.

of these nuclei, measured variously by β nuclear magnetic resonance, β nuclear quadrupole resonance, and atomic or molecular beam measurements [8]. The exceptions are ^{7}Be, ^{9}B (the narrow resonance noted above), and ^{9}C. Experimental quadrupole moments for members of the mirror pairs considered here, as evaluated in Ref. [8], are summarized in Table I. Uncertainties range from the order of 10% to less than 1% (although the signs of some of these quadrupole moments are experimentally undetermined or uncertain). These experimental values provide the basis for stringent comparisons with theoretical predictions.

The quadrupole moments of both members of the pair are thus experimentally known in the case of the $A = 8$, 11, 12, and 13′ mirror pairs. For these, the ratio is also given for reference in Table I. For consistency in defining the ratios, we always take the ratio of the quadrupole moment for the proton-rich ($Z > N$) nuclide to that of the neutron-rich ($Z < N$) nuclide.

III. *AB INITIO* PREDICTIONS FOR QUADRUPOLE MOMENT MIRROR RATIOS

A. Mirror nuclide quadrupole moments: $A = 7$

Let us first consider the $A = 7$ mirror pair in detail. Here we define the NCCI calculations, illustrate the challenges associated with predicting quadrupole moments directly from such calculations, and then explore the rationale for instead considering their ratios. We will then, in subsequent subsections, survey the results for the remaining mirror pairs, both odd-mass (Sec. III B) and odd-odd (Sec. III C).

The NCCI approach [23] is based on diagonalizing the nuclear many-body Hamiltonian in a basis of antisymmetrized product states (Slater determinants) constructed from some single particle basis, most commonly harmonic oscillator orbitals. Actual calculations must be carried out in a finite, truncated basis. The energies and other observables thereby obtained are only approximations to those which would be obtained in the full many-body space. However, by systematically expanding the basis, it is in principle possible to approach the full-space values to any desired degree of accuracy. The actual accuracy which can be reached is subject to computational

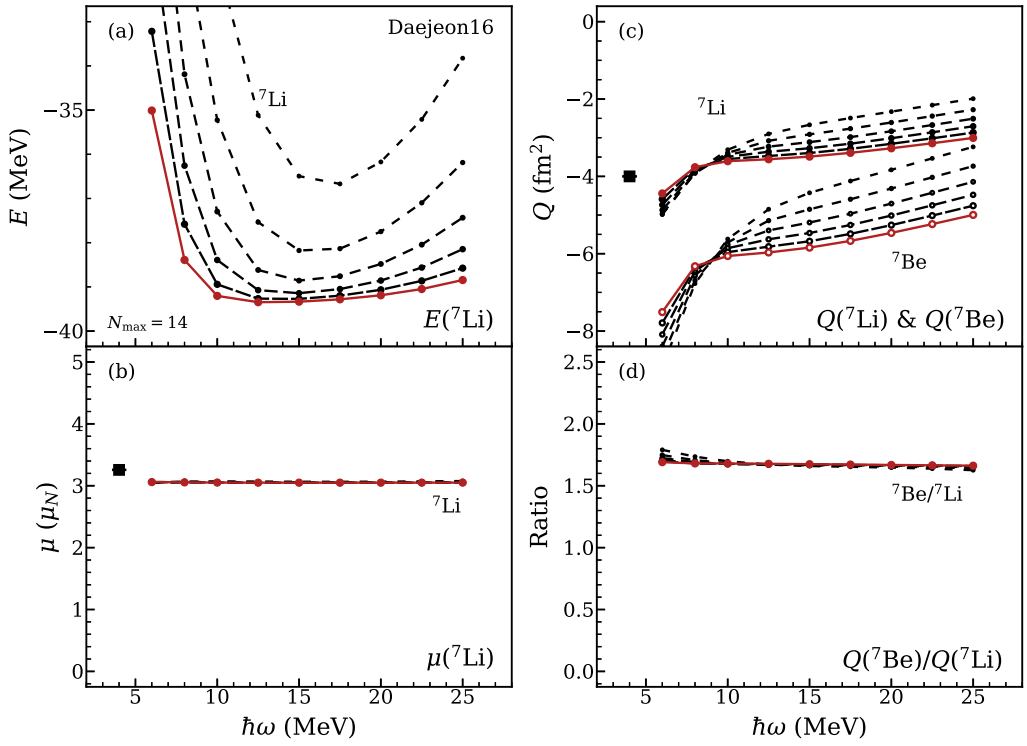

FIG. 2. Convergence of *ab initio* NCCI calculations for the $A = 7$ mirror nuclides, with the Daejeon16 interaction: (a) the $3/2^-$ ground state energy for ^{7}Li, (b) the ground state magnetic dipole moment μ for ^{7}Li, (c) the ground state electric quadrupole moment Q for ^{7}Li (filled symbols) and ^{7}Be (open symbols), and (d) the ratio of the quadrupole moment for ^{7}Be to that of ^{7}Li. Calculated values are shown as functions of the basis parameter $\hbar\omega$, for successive even value of $N_{\max}$ (increasing symbol size and longer dashing), from $N_{\max} = 4$ (short dashed curves) to 14 (solid curves). Experimental values are also shown for the ^{7}Li magnetic dipole [42] and electric quadrupole [8] moments (squares, at left).

limitations on the problem size.

The NCCI basis states may be organized according to the number N_{ex} of oscillator excitations relative to the lowest Pauli-allowed filling of oscillator shells. The many-body basis is then, for practical reasons (*e.g.*, Ref. [44]), conventionally truncated to a maximum number $N_{\max}$ of oscillator excitations above the lowest filling (*i.e.*, to $N_{\mathrm{ex}} \leq N_{\max}$). The space spanned by the many-body basis also depends upon the oscillator length b of the underlying oscillator orbitals, commonly expressed in terms of the corresponding oscillator energy $\hbar\omega$ [45]. The full-space values for observables should be recovered as $N_{\max}$ approaches infinity, in which limit the calculated values also become independent of $\hbar\omega$.

Consider first the calculated energy eigenvalue for the ground state of ^{7}Li, shown in Fig. 2(a), for the Daejeon16 interaction. (The present calculations are obtained using the M-scheme NCCI code MFDn [46, 47].) Each curve represents calculations at fixed truncation $N_{\max}$ ($N_{\max} = 4$ to 14, even), for varying $\hbar\omega$. The calculated ground state energy is variationally bounded below by the full-space value. An approach to convergence is evident in the curves becoming successively closer together (independent of $N_{\max}$) and flatter (independent of $\hbar\omega$), as they approach the variational lower bound, such that the highest $N_{\max}$ curves lie nearly atop each other at the scale shown. A qualitatively similar convergence pattern is obtained for other choices of interaction, although the rate of convergence and the location (in $\hbar\omega$) of the variational minimum in each curve will in general differ.

The quality of convergence in an NCCI calculation depends upon the observable (and states) under consideration. For instance, magnetic dipole ($M1$) observables, which are largely sensitive to the angular momentum structure of the wave functions, may attain very rapid convergence, as illustrated for the calculated dipole moment of ^{7}Li in Fig. 2(b). (The calculated magnetic dipole moment is also reasonably consistent with the experimental value [42].) In contrast, electric quadrupole ($E2$) observables, which are more sensitive to the radial behavior (the "tails" of the wave functions are amplified by the r^2 radial dependence of the quadrupole operator), are comparatively difficult to converge.

Indeed, the calculated quadrupole moment for the ^{7}Li ground state, shown by the filled symbols in Fig. 2(c), depends strongly upon $\hbar\omega$ at fixed $N_{\max}$, especially for low $N_{\max}$, and continues to vary steadily with increasing $N_{\max}$. Note that the overall trend of each curve with respect to $\hbar\omega$, from asymptotically large magnitude as $\hbar\omega \to 0$ to asymptotically small magnitude as $\hbar\omega \to \infty$,

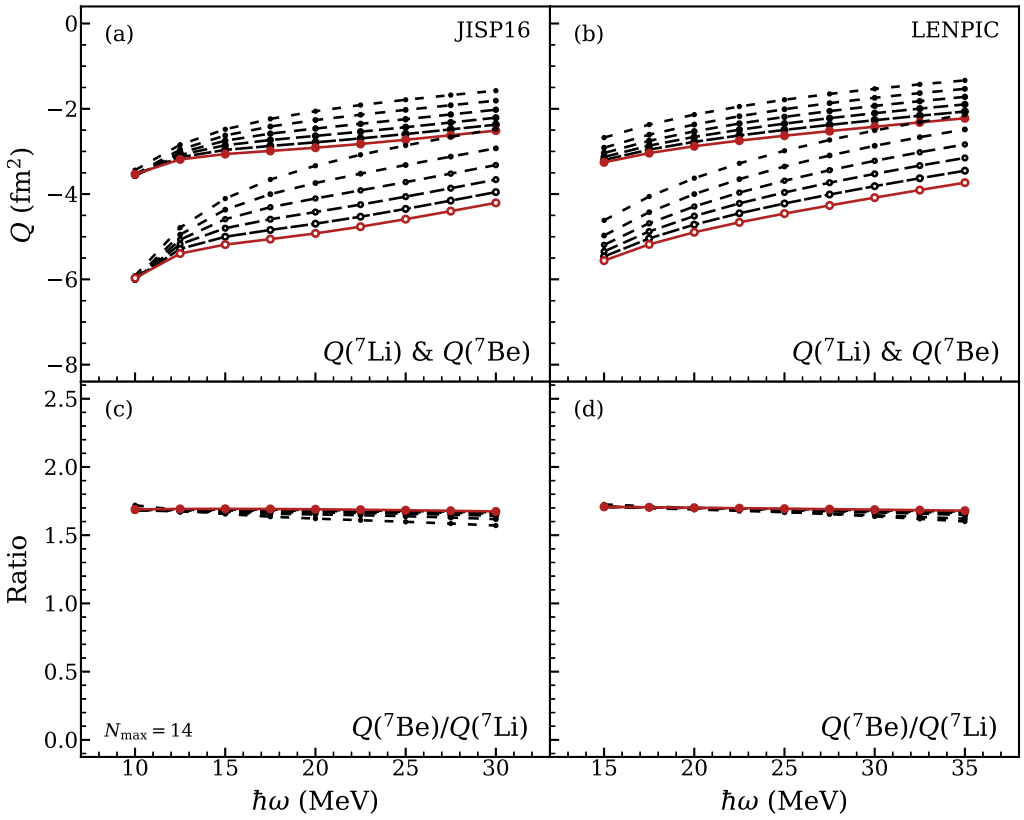

FIG. 3. Quadrupole moments for the $A = 7$ mirror nuclides, calculated with the JISP16 (left) and LENPIC (right) interactions: (top) quadrupole moments for ^{7}Li (filled symbols) and ^{7}Be (open symbols), and (bottom) the ^{7}Be to ^{7}Li mirror ratio. Calculated values are shown as functions of the basis parameter $\hbar\omega$, for successive even values of $N_{\max}$ (increasing symbol size and longer dashing), from $N_{\max} = 4$ (short dashed curves) to 14 (solid curves).

is simply a consequence of the dependence on $\hbar\omega$ of the length scale of the basis functions. For a single oscillator basis function, the quadrupole moment scales as $Q \propto b^2$, where $b \propto (\hbar\omega)^{-1/2}$, and is thus inversely proportional to $\hbar\omega$.

Encouragingly, there does appear to be some progress towards convergence, with increasing $N_{\max}$, in the calculated ^{7}Li quadrupole moment. In particular, note the significant flattening (or "shouldering") of the curves at high $N_{\max}$, as well as some degree of compression of successive curves against each other with increasing $N_{\max}$. There is also a narrow region, around $\hbar\omega \approx 9$ MeV, where the curves cross each other, and therefore locally approach $N_{\max}$ independence. Such crossings have been suggested as a heuristic indicator of convergence [48–50] (although, in general, such crossings drift with $N_{\max}$ [51] and are thus of limited use in estimating the converged value). It is perhaps reassuring that, in the shoulder region, the calculated values of the quadrupole moment appear to be roughly consistent with, and approaching, the experimental value. Nonetheless, it is less than obvious how to extract a firm quantitative value for the predicted quadrupole moment in the full, untruncated many-body problem (at least without significant further assumptions about the nature of the convergence, *e.g.*, as in Ref. [52]).

The calculated quadrupole moment for the mirror nuclide ^{7}Be, shown by the open symbols in Fig. 2(c), shares a similarly encouraging approach to convergence but is likewise insufficiently converged to provide a firm quantitative prediction. Indeed, the two quadrupole moments in Fig. 2(c) have similar convergence trends, differing primarily in overall normalization.

Herein lies the motivation for considering ratios. The error introduced by basis truncation may largely cancel in the ratio of these quadrupole moments, providing a more robustly converged prediction for their ratio. Such cancellation and robust convergence has already been noted for the ratio between the mirror $E2$ transitions ($3/2^- \rightarrow 1/2^-$) in these two nuclei [26] (see Fig. 6 of Ref. [26]). Indeed the ratio of the calculated quadrupole moments for ^{7}Be and ^{7}Li, shown in Fig. 2(d), is seen to be largely independent of $N_{\max}$ and $\hbar\omega$.

It is informative to compare the convergence behavior obtained for different choices of interaction, derived by different procedures. The Daejeon16 interaction [27] is a comparatively "soft" interaction. It is based on the two-body part of the Entem-Machleidt (EM) N^{3}LO chiral EFT interaction [53], softened via a similarity renor-

malization group (SRG) transformation [54] to enhance convergence, and then adjusted via a phase-shift equivalent transformation to better describe light nuclei with $A \leq 16$ (see Ref. [55] for comparison with experiment). The earlier JISP16 interaction [28] is derived instead from nucleon-nucleon scattering data by J-matrix inverse scattering, then similarly adjusted via phase-shift equivalent transformations to data for nuclei with $A \leq 16$ (see Ref. [24] for comparison with experiment). Alternatively, the LENPIC interaction [29, 30] is a newer chiral EFT interaction, developed with an ultraviolet regularization scheme designed to minimize finite-cutoff artifacts. We consider the two-body part of this interaction at N^{2}LO, which provides a reasonable description of nuclear observables without adjustment [56, 57]. Here we take it with a semi-local coordinate-space regulator ($R = 1\,\mathrm{fm}$), and in its "bare" form, *i.e.*, without subsequent SRG transformation.

The calculated $A = 7$ quadrupole moments, and their ratio, for the JISP16 and LENPIC interactions are shown in Fig. 3. (For each interaction, we consider calculations in an $\hbar\omega$ range centered on the approximate location of the variational minimum of the ground state energy, for calculations with that interaction.) The calculated quadrupole moments themselves show less indication of convergence than for Daejeon16 [Fig. 2(c)]. There is a hint of shouldering in the calculated quadrupole moments for JISP16 [Fig. 3(a)], which cross at $\hbar\omega \lesssim 10\,\mathrm{MeV}$, but little suggestion of convergence at all for the unsoftened LENPIC interaction [Fig. 3(b)].

Nonetheless, the mirror ratio of quadrupole moments [Fig. 3(c,d)] is again robustly converged, much as for the Daejeon16 interaction [Fig. 2(d)]. We observe close quantitative agreement between the predictions for the $A = 7$ quadrupole moment ratio obtained with the Daejeon16, JISP16, and LENPIC interactions.

Within the $A = 7$ mirror pair, the quadrupole moment of ^{7}Be is unmeasured, and thus experiment does not provide a test of the NCCI predictions. Rather, the robust NCCI prediction of the ratio (approximately $+1.7$), taken in conjunction with the measured quadrupole moment of $-4.0\,\mathrm{fm}^2$ for ^{7}Li (Table I), provides a concrete prediction of approximately $-6.8\,\mathrm{fm}^2$ for the unmeasured ^{7}Be quadrupole moment.

B. Odd-mass mirror pairs

Let us now consider the *ab initio* predictions for the quadrupole moments and their ratios for the remaining p-shell mirror pairs ($A > 7$). The calculated quadrupole moments for both members of each mirror pair are overlaid in the upper member of each pair of panels in Fig. 4, demonstrating the convergence behavior with respect to $N_{\max}$ and $\hbar\omega$. Then the calculated ratio is shown in the lower member of each pair of panels in Fig. 4. We again focus on the calculations with the Daejeon16 interaction for detailed analysis (comprehensive tabulations of the calculated quadrupole moments for all three interactions are provided in the Supplemental Material [58]). The experimental values are indicated for comparison, where available, in Fig. 4, with the caveat that signs are not always experimentally determined (see Table I). While calculations for all of the mirror pairs are shown in Fig. 4, we discuss first the remaining odd-A nuclides, before turning to the odd-odd nuclides below in Sec. III C.

To provide a concise, though less nuanced, global comparison of results for the quadrupole moment ratios, for all mirror pairs and for all choices of interaction, it is helpful to take a slice at fixed $\hbar\omega$ through the convergence results, considering only the $N_{\max}$ dependence. A natural choice for $\hbar\omega$ is again the approximate location of the variational minimum of the ground state energy [recall the ^{7}Li energy calculations in Fig. 2(a)]. The exact position of this minimum varies with nuclide and with $N_{\max}$, but for Daejeon16 we standardize on $\hbar\omega = 15\,\mathrm{MeV}$ as a reasonable estimate, and similarly we adopt 20 MeV for JISP16 and 25 MeV for LENPIC. Then we are able to make side-by-side numerical comparisons of the $N_{\max}$-dependence of the calculated quadrupole moment ratios, as shown in Fig. 5. The calculated ratio for the $A = 7$ mirror pair, discussed above in Sec. III A, may be found at far left [Fig. 5(a)].

Furthermore, for the lighter nuclides ($A \leq 9$), *ab initio* results [39] for the quadrupole moments have previously been obtained by Green's function Monte Carlo (GFMC) methods [59], in calculations based on the Argonne v_{18} (AV18) two-nucleon [60] and Illinois-7 (IL7) three-nucleon [61] potentials. The predicted quadrupole moments are quoted for reference in Table I. For the $A = 7$ pair, the resulting ratio, shown as a cross in Fig. 5(a), is closely aligned with the present predictions, to within the GFMC statistical uncertainties.

In the $A = 9$ mirror pair (^{9}Be and ^{9}B), the calculated quadrupole moments themselves [Fig. 4(b)] show a trend towards convergence with increasing $N_{\max}$, much as for the $A = 7$ pair above [Fig. 2(c)] (when comparing, note the opposite overall sign of the quadrupole moments, between $A = 7$ and $A = 9$). The "shoulder" in the calculated quadrupole moment for ^{9}Be (filled symbols) suggests a value roughly consistent with experiment. For ^{9}B (open symbols), the turnover in the calculated quadrupole moment for $\hbar\omega \lesssim 10\,\mathrm{MeV}$ appears to reflect a more general breakdown in the ability of the calculation to preserve the excitation spectrum of $3/2^-$ states at low $\hbar\omega$ (bases with excessively low $\hbar\omega$ have an excessively long oscillator length scale).

While these individual calculated quadrupole moments still exhibit significant basis dependence, the calculated ratio [Fig. 4(e)] is largely independent of $\hbar\omega$ and $N_{\max}$, even at comparatively low $N_{\max}$, for $\hbar\omega \gtrsim 10\,\mathrm{MeV}$. (The failure below $\hbar\omega \approx 10\,\mathrm{MeV}$ is perhaps not surprising, given the more general breakdown noted above.) From Fig. 5(c), it is seen that the Daejeon16, JISP16, and LENPIC interactions yield consistent predictions for the quadrupole moment ratio, furthermore consis-

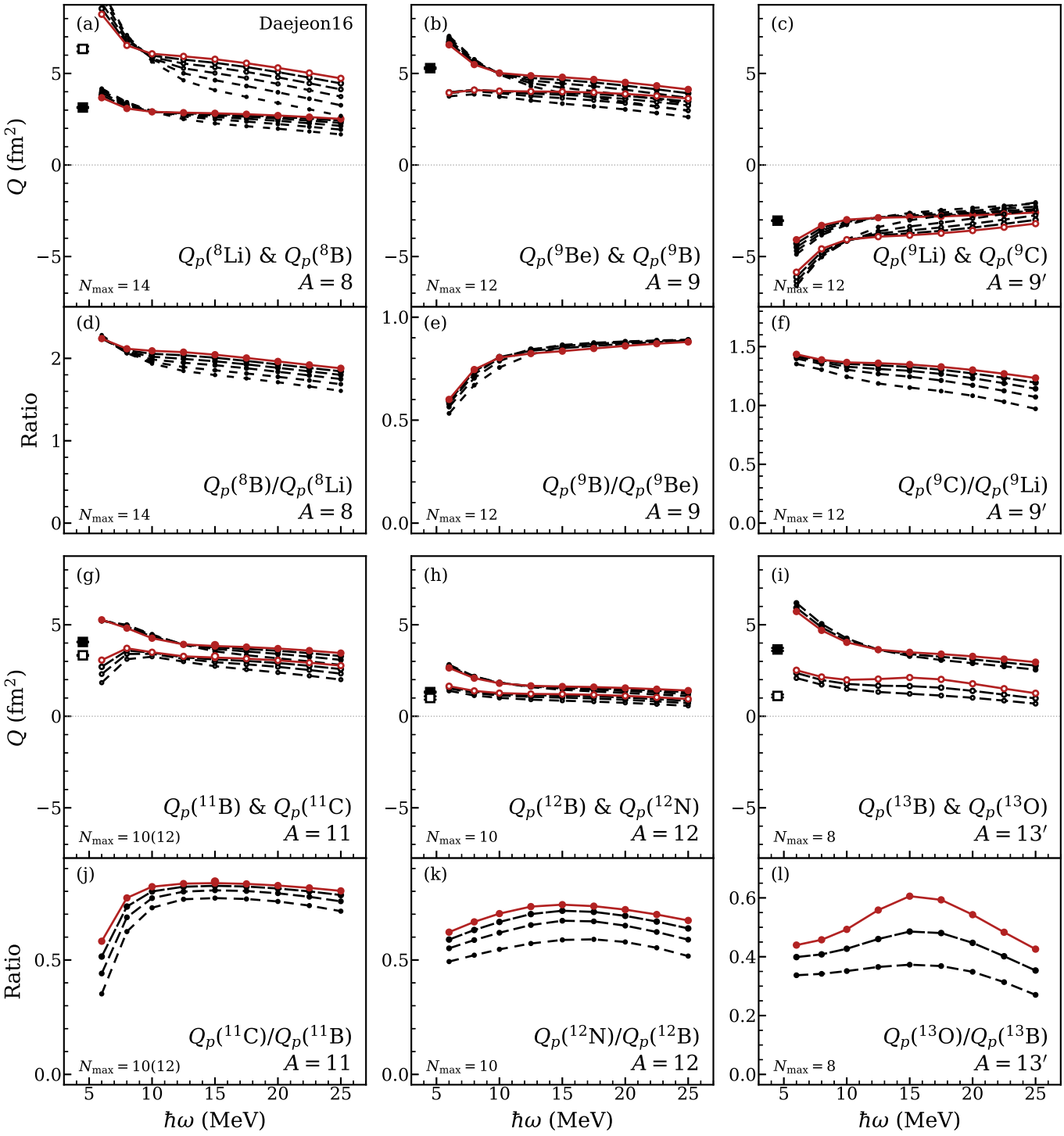

FIG. 4. Quadrupole moments for p-shell mirror nuclides (upper member of each pair of panels), for $A > 7$, and the ratio of quadrupole moments across each mirror pair (lower member of each pair of panels), calculated with the Daejeon16 interaction. Calculated values (circles) are shown as functions of the basis parameter $\hbar\omega$, for successive even values of $N_{\max}$ (increasing symbol size and longer dashing), from $N_{\max} = 4$ (short dashed curves) to the maximum value for that mirror pair (solid curves), indicated at bottom. Quadrupole moments for the neutron-rich ($Z < N$) nuclides are shown with filled symbols, and those for the proton-rich ($Z > N$) nuclides with open symbols. Also shown are the experimental quadrupole moments [8] (squares) from Table I (some signs experimentally undetermined).

tent with the GFMC AV18+IL7 results. The stable and interaction-independent NCCI prediction of the ratio (in the range of approximately +0.80 to +0.85), taken in conjunction with the measured quadrupole moment of $+5.3\,\mathrm{fm}^2$ for ^{9}Be (Table I), provides a prediction of about $+4.2\,\mathrm{fm}^2$ to $+4.5\,\mathrm{fm}^2$ for the unmeasured ^{9}B quadrupole moment.

In the $A = 9'$ mirror pair (^{9}Li and ^{9}C), the convergence of the quadrupole moment ratio is less robust. The moments themselves [Fig. 4(c)] again show signs of shouldering, and for ^{9}Li (filled symbols) there is again general consistency with the experimental value. While the quadrupole moment ratio [Fig. 4(f)] would also appear to be approaching convergence, this occurs more slowly than in the previous cases. Consequently, one would be hard put to make an estimate except that the value appears likely to be between 1.3 and 1.5 with Daejeon16. The different interactions [Fig. 5(d)] yield a spread of $\sim 10\%$ in the predicted ratio, in the calculations at the highest $N_{\max}$. However, this spread also seems to be decreasing with increasing $N_{\max}$, so it might not reflect a true difference in predictions for the different interactions.

The direction of convergence of the NCCI predicted ratios for the $A = 9'$ mirror pair is such as to bring them towards consistency with the GFMC AV18+IL7 result. Note the larger statistical uncertainties obtained in the GFMC calculations for the $A = 9'$ mirror nuclides, in this case accompanying the poorer convergence of the NCCI calculations.

Note that ^{9}C is a comparatively weakly-bound nucleus, with its ground state only $\sim 1.3\,\mathrm{MeV}$ below the $^8\mathrm{B} + p$ breakup threshold [35], relative to its mirror nuclide ^{9}Li, which is bound by $\sim 4.1\,\mathrm{MeV}$ against the analogous $^8\mathrm{Li} + n$ breakup channel. This difference could ostensibly introduce greater sensitivities in calculating the long-range behavior of the wave function, *e.g.*, through an extended proton single-particle wave function. Yet, binding energy alone clearly does not suffice to explain the differences, as ^{9}B is $\sim 0.3\,\mathrm{MeV}$ *above* the $^8\mathrm{Be} + p$ threshold, and comparatively rapid convergence was obtained above. (For that matter, in the $A = 7$ pair considered above, ^{7}Be is bound by not much more, $\sim 1.6\,\mathrm{MeV}$ [34], although this is against a cluster breakup mode, $^3\mathrm{He} + {}^4\mathrm{He}$, rather than separation of a single nucleon.)

The $A = 11$ pair (^{11}C and ^{11}B) presents a comparatively simple picture of convergence. For both members of the pair, the quadrupole moments themselves [Fig. 4(g)] both show some evidence of shouldering, consistent with the experimental value. In the calculations for Fig. 4(g), full scans over $\hbar\omega$ are carried out through $N_{\max} = 10$. However, an $N_{\max} = 12$ calculation, currently just computationally feasible, is included at the variational minimum $\hbar\omega$ [hence the indication of $N_{\max}$ as "10(12)" in Fig. 4(g,j) and subsequent figures]. The now-familiar turnover at low $\hbar\omega$ ($\lesssim 10\,\mathrm{MeV}$), is observed for the ^{11}C quadrupole moment. These nuclei, incidentally, are the most bound of the mirror pairs considered here, by over 11 MeV for ^{11}B and over 7 MeV for ^{11}C [38].

The ratio of quadrupole moments for $A = 11$ [Fig. 4(j)] is rapidly converging, approaching a value in the vicinity of 0.8. It appears that a slightly higher value may be obtained with the Daejeon16 interaction than with the others [Fig. 5(d)], but all lie within a range of 0.7 to 0.9, closely consistent with experiment.

Finally, among the odd-mass nuclei, the $A = 13'$ pair (^{13}O and ^{13}B) presents a qualitatively different convergence behavior. Examining the calculated quadrupole moments [Fig. 4(i)], we see that those for ^{13}B (filled circles) exhibit the familiar shouldering and again tend toward a value consistent with experiment. However, the corresponding curves for ^{13}O (open circles) bulge upwards with increasing $N_{\max}$. At $\hbar\omega = 15\,\mathrm{MeV}$, the value approximately doubles between $N_{\max} = 4$ and $N_{\max} = 8$. These calculated values already exceed the experimental quadrupole moment and continue to move away with increasing $N_{\max}$. The quadrupole moment ratio [Fig. 4(l)] likewise rapidly grows past the experimental ratio [Fig. 5(g)]. (The ratios obtained with the JISP16 and LENPIC interactions similarly grow steadily, though not as rapidly, with increasing $N_{\max}$ [58].)

In a shell-model picture, the $A = 13'$ nuclei are semimagic. The protons in ^{13}O form a closed major oscillator shell in a $0\hbar\omega$ configuration. Thus, the proton quadrupole moment in ^{13}O must vanish at $N_{\max} = 0$. (The neutron quadrupole moment in ^{13}B must similarly vanish at $N_{\max} = 0$.) Any nonzero value of the ratio of the ^{13}O quadrupole moment to the ^{13}B quadrupole moment must come from the introduction of $2\hbar\omega$ or higher configurations into the NCCI wave function, as $N_{\max}$ increases from 0. Thus, the semimagic nature of ^{13}O at least explains why the convergence behavior for the proton quadrupole moment [open symbols in Fig. 4(i)] must qualitatively differ from the other cases considered.

However, semimagicity does not immediately explain why the calculated quadrupole moment continues to grow towards excessively large values with increasing $N_{\max}$. Experimentally, the ground state of ^{13}O is only $\sim 1.5\,\mathrm{MeV}$ below the breakup threshold ($^{12}\mathrm{N} + p$) [37], so one might suspect sensitivity to long-range behavior of the wave function, but the same convergence pattern is calculated for the neutron quadrupole moment in ^{13}B, which is more tightly bound, by $\sim 4.9\,\mathrm{MeV}$ with respect to $^{12}\mathrm{B} + n$. An alternative explanation in terms of shape coexistence is noted below (Sec. V).

C. Odd-odd mirror pairs

Returning now to the odd-odd nuclides, let us consider the $A = 8$ pair (^{8}Li and ^{8}B). Although both calculated quadrupole moments [Fig. 4(a)] ultimately display the familiar shouldering behavior for high $N_{\max}$, at values roughly consistent with experiment, the convergence for ^{8}B (open circles) is notably slower than for most of

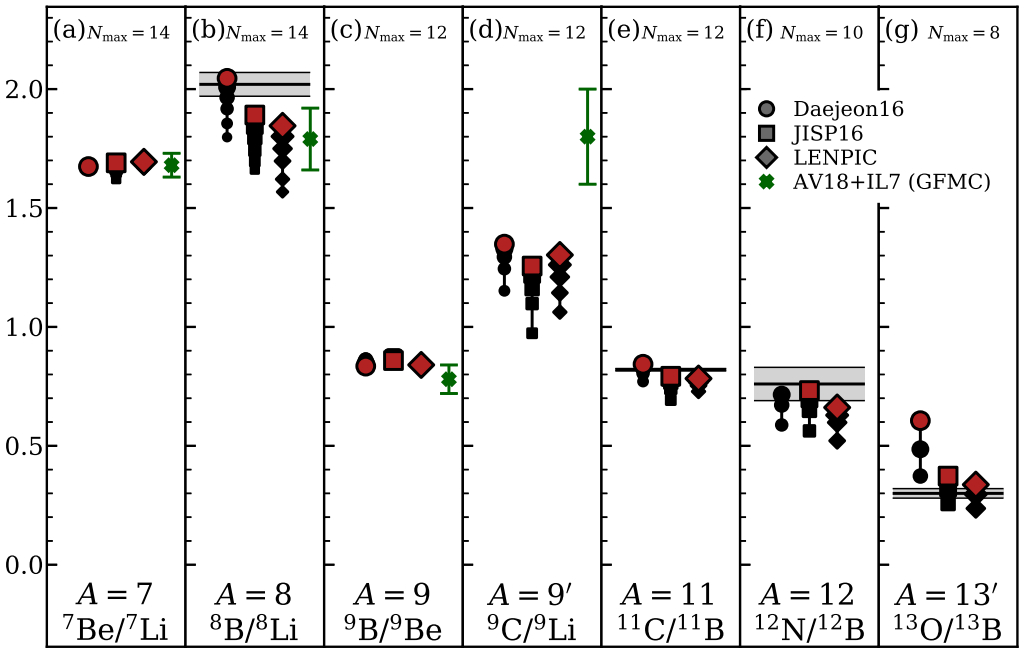

FIG. 5. Quadrupole moment mirror ratios for p-shell mirror pairs, obtained with the Daejeon16 (circles), JISP16 (squares), and LENPIC (diamonds) interactions, at fixed $\hbar\omega$ (15 MeV, 20 MeV, and 25 MeV, respectively, for the three interactions). Calculated values are shown for successive even values of N_{max} (increasing symbol size), from $N_{max} = 4$ to the maximum value for that mirror pair, indicated at top. Also shown (from Table I) are the GFMC AV18+IL7 predictions [39] (crosses) and ratios of experimental quadrupole moments [8] (horizontal line and error band), where some signs are experimentally undetermined.

the others in Fig. 4 (note the wider spread in calculated curves). Such slow convergence is perhaps not surprising given the expected proton halo structure of ^{8}B [6, 7, 62], and thus extended tail region to the proton distribution. Here it is worth noting the ^{8}B ground state is extremely weakly bound, compared to any of the other (bound) nuclei considered here, by only ~ 0.13 MeV with respect to ^{7}Be$+p$ breakup [35], while ^{8}Li, the neutron-rich member of this mirror pair, is bound by ~ 2.0 MeV with respect to ^{7}Li $+ n$ breakup.

The ratio of quadrupole moments for $A = 8$ [Fig. 4(d)] is therefore also slow to converge. Although the curves at high N_{max} form shoulders, or plateaus, these plateaus continue to move slowly but steadily upward with increasing N_{max}. The bulk of this N_{max} dependence comes from the ^{8}B quadrupole moment.

The resulting ratios obtained with all three interactions [Fig. 5(b)] are in the vicinity of the experimental ratio. The Daejeon16 result for the ratio is just growing past the experimental value, at the highest N_{max} calculated, while the JISP16 and LENPIC results are still approaching it. The continued basis sensitivity precludes more precise comparison. Here again, as for the $A = 9'$ pair above (Sec. III B), the slow convergence of the ratio in the NCCI calculations is accompanied by a large GFMC statistical uncertainty.

For the $A = 12$ pair (^{12}B and ^{12}N), the experimental quadrupole moments are markedly smaller in magnitude (by a factor of $\sim$ 3–6) than those considered above, except for the semi-magic ^{13}O. Consider, then, the calculated quadrupole moments [Fig. 4(h)]. Those for ^{12}B (filled circles) show shouldering, and would appear to be converging, but tend towards a value perhaps as much as 50% higher than the experimental value. Those for ^{12}N (open circles), while also showing some sort of shouldering, only gradually come closer together with increasing N_{max}, showing no clear sign of convergence, but have also already grown past the experimental value.

Given the different convergence patterns for the individual quadrupole moments, the calculated ratio [Fig. 4(k)] for the $A = 12$ pair is consequently also comparatively slow to converge, but the calculated values do appear to form a roughly geometric progression, approaching a ratio $\sim$ 0.8. There is a spread of $\sim$ 10% among the calculated ratios obtained with the three different interactions [Fig. 5(f)], at the highest N_{max}, but all would seem on course to yield values within the uncertainties of the experimental ratio.

The ^{12}N ground state is bound by only ~ 0.60 MeV with respect to ^{11}C $+ p$ breakup [36]. One might be tempted to attribute slow convergence for the $A = 12$ quadrupole moment ratio, and likewise for the $A = 8$ ratio above, to this weak binding of the proton-rich member of the pair, which may well contribute. However, odd-odd nuclei have notoriously complicated spectra [3] even when strongly bound, and a comparatively high level density near the ground state is conducive to mixing. Arguments to this effect for ^{8}Li, in particular, may be made [63] on

the basis of the appearance of approximately degenerate ground states in an Elliott SU(3) [32, 33] symmetry description.

IV. MIRROR SYMMETRY BREAKING

Let us now return to the question of the extent to which proton and neutron quadrupole moments are actually related by mirror symmetry across a mirror pair. In the present *ab initio* calculations, the isospin is found to be a "good" quantum number, with isospin $T = |T_z|$, to high precision, for all the calculated ground state wave functions. Wave function components with $T > |T_z|$ contribute, *e.g.*, $\lesssim 10^{-4}$ to the norm of the calculated ground state wave function for ^{7}Li.[1]

While the observation that each ground state in the mirror pair has good isospin is sufficient to exclude isospin *mixing*, it does not in itself establish isospin (or mirror) *symmetry* between the states. Under isospin symmetry, an isobaric multiplet consists of states which not only share the same T, but also, more specifically, have wave functions related by successive application of the isospin raising and lowering operators. (For mirror states, the wave functions are, equivalently, related by a rotation by π in isospin space.) Even if the isospin violating part of the many-body Hamiltonian does not significantly induce mixing of different isospins in the wave function, it might still induce mixing within the $T = |T_z|$ sector of the many-body space in a way which varies with T_z, and thus differs across the analog states. This would be apparent in a violation of the isospin (or mirror) symmetry predictions for observables. For mirror quadrupole moments in particular, there may be deviations from equality between the neutron quadrupole moment Q_n of one mirror state and the proton quadrupole moment Q_p of the other.

We have thus far considered the ratio of the proton (electric) quadrupole moments across the mirror pair (Sec. III), partly as an experimental observable in its own right to provide a test for *ab initio* theory, but partly also on the premise it may be taken as a proxy for the ratio Q_n/Q_p within a single nuclide, to directly reflect proton-neutron structure in that nuclide. If we denote the quadrupole moment in the "mirror" nuclide by $\tilde{Q}_p$, our specific interest is thus in how well the mirror ratio $\tilde{Q}_p/Q_p$ approximates Q_n/Q_p. These ratios are related by

$$\frac{\tilde{Q}_p}{Q_p} = \left(\frac{\tilde{Q}_p}{Q_n}\right)\left(\frac{Q_n}{Q_p}\right), \tag{1}$$

where the deviation of the first factor, $\tilde{Q}_p/Q_n$, from unity thus measures how much error is introduced by taking the mirror ratio as a proxy for the neutron-proton ratio. Based on the present wave functions from NCCI calculations, we therefore explicitly calculate $\tilde{Q}_p/Q_n$ and look for deviations from unity.

Let us start with the $A = 7$ mirror pair, and explore the dependence of the calculated $\tilde{Q}_p/Q_n$ — in this case, $Q_p(^7\mathrm{Be})/Q_n(^7\mathrm{Li})$ — on the basis parameters of the truncated calculation. Taking first the results for the Daejeon16 interaction [Fig. 6(a)], the deviations from unity found in the present calculations, at $\lesssim 5\%$, might seem modest from a practical perspective, in terms of the precision we may desire in extracting the quadrupole moment ratio. However, the calculated ratio shows little indication of convergence with respect to $N_{\max}$. While the $\hbar\omega$-dependence of the curves is modest, with a gentle peak near $\hbar\omega = 10\,\mathrm{MeV}$, curves for successive $N_{\max}$ are nearly equidistant, giving larger values of the ratio for increasing $N_{\max}$. Assuming this trend continues, the present NCCI calculations provide only a lower bound on the deviation from mirror symmetry which would be obtained (in the full, untruncated many-body problem) for the quadrupole moments, assuming the Daejeon16 interaction.

The interactions used in *ab initio* calculations have an isospin violating portion which is either simplified outright (to the Coulomb interaction) or subject to notable uncertainties in the nuclear part [64]. Both the Daejeon16 and JISP16 interactions are purely isoscalar, before inclusion of the Coulomb interaction, which is thus the only source of isospin symmetry violation. (The proton-neutron mass difference is commonly neglected in NCCI calculations [44, 65, 66].) In contrast, the LENPIC interaction explicitly includes isospin violation from the strong interaction (*e.g.*, Ref. [64]). It is not *a priori* obvious how this might influence the deviations from mirror symmetry in the quadrupole moment.

The violation of mirror symmetry in the $A = 7$ pair is compared across interactions in Fig. 6 (top). The scale of the calculated deviations, for any given $N_{\max}$ and $\hbar\omega$, is found to be comparable across the Daejeon16 [Fig. 6(a)] and JISP16 [Fig. 6(b)] interactions, not surprisingly given their shared reliance on the Coulomb interaction as their isospin symmetry breaking part, and marginally smaller for the LENPIC interaction [Fig. 6(c)]. However, there is no obvious gross qualitative difference across interactions, and any detailed quantitative comparison of these unconverged calculations is meaningless in light of the different convergence rates for calculations with different interactions.

Proceeding to the remaining mirror pairs ($A > 7$), we focus for purposes of illustration on the results obtained

[1] The isospin contamination is most simply ascertained by evaluating the expectation value of $\mathbf{T}^2$ within the many-body wave function. For a state which is an admixture of $T = |T_z|$ and $T = |T_z| + 1$ components, $|\Psi\rangle = \alpha|\Psi_{T=|T_z|}\rangle + \beta|\Psi_{T=|T_z|+1}\rangle$, with probabilities α^2 and β^2, respectively, it is readily verified that the $T = |T_z| + 1$ component contributes with probability $\beta^2 = [2(|T_z|+1)]^{-1}[\langle\mathbf{T}^2\rangle - |T_z|(|T_z|+1)]$. More generally, if components with multiple $T \geq |T_z|$ contribute, this two-component estimate places an upper bound on the total $T > |T_z|$ contribution.

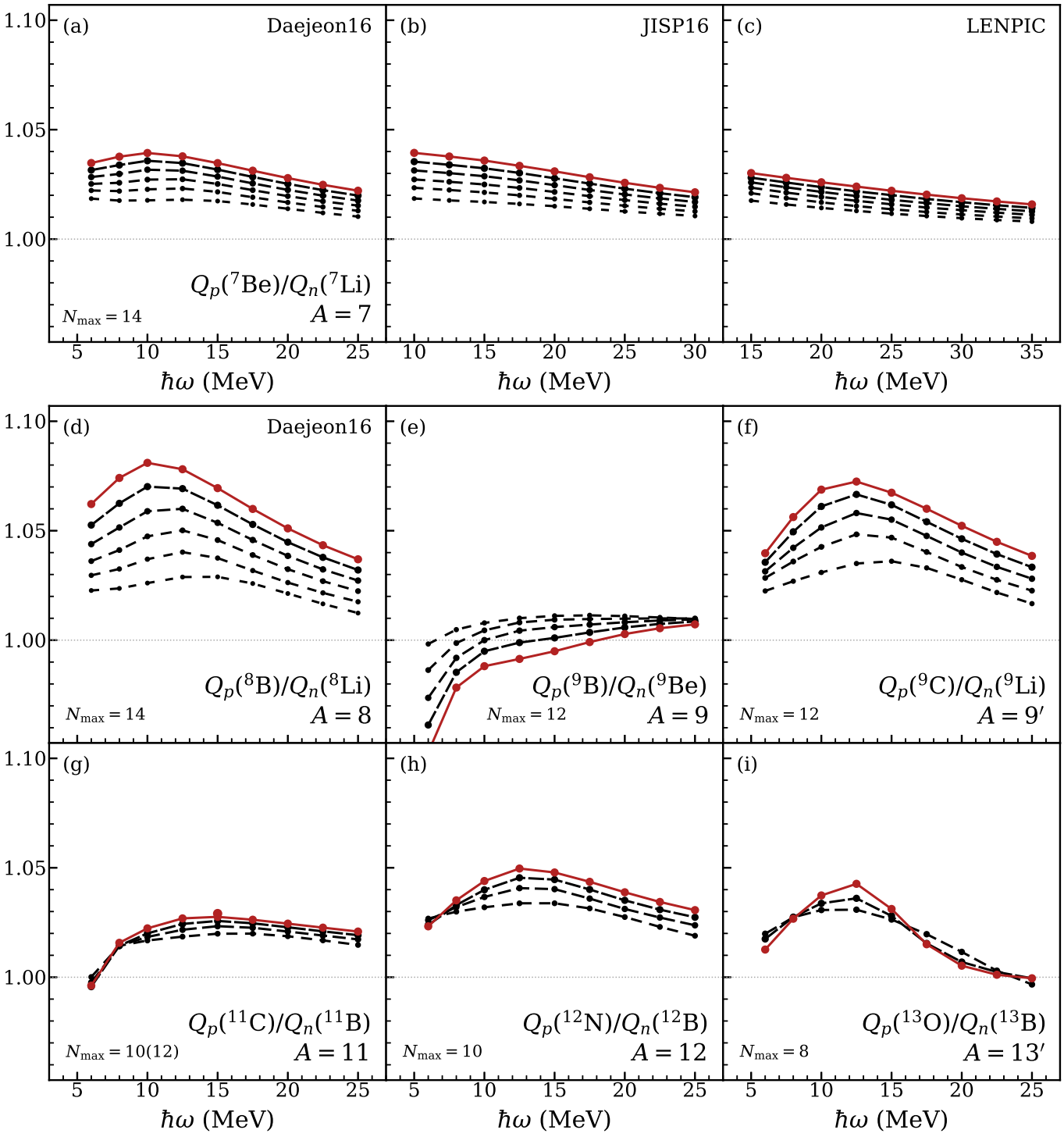

FIG. 6. Relation between Q_n (in the proton-rich nuclide) to its mirror proxy Q_p (in the neutron-rich nuclide), represented as the ratio $\tilde{Q}_p/Q_n$ (see text): (top) for the $A = 7$ mirror pair with Daejeon16, JISP16, and LENPIC interactions and (bottom) for the $A > 7$ mirror pairs with the Daejeon16 interaction. Calculated values (circles) are shown as functions of the basis parameter $\hbar\omega$, for successive even values of $N_{\max}$ (increasing symbol size and longer dashing), from $N_{\max} = 4$ (short dashed curves) to the maximum value for that mirror pair (solid curves), indicated at bottom.

with the Daejeon16 interaction. (Comprehensive tabulations for all three interactions are again provided in the Supplemental Material [58].) The convergence properties of the calculated $\tilde{Q}_p/Q_n$ are shown in Fig. 6 (bottom). As in the $A = 7$ example above, we again take the "nuclide of interest" for calculating Q_n/Q_p, in (1), to be the neutron-rich ($Z < N$) member of the mirror pair, and the "mirror nuclide" providing the "proxy" value $\tilde{Q}_p$ to be the proton-rich ($Z > N$) member. To provide a global comparison across interactions, we also present the results for all three interactions as functions of $N_{\max}$ for fixed $\hbar\omega$ in Fig. 7 (that is, in the same spirit as Fig. 5 above).

For all mirror pairs, the calculated deviations of $\tilde{Q}_p/Q_n$ from unity, as seen in Figs. 6 or 7, may again seem modest, at $< 10\%$. But again nonconvergence with respect to $N_{\max}$ is the norm. Following the same order of discussion as in Sec. III, let us proceed first through the odd-mass nuclides, then return to the odd-odd nuclides.

For $A = 9$ [Figs. 6(e) and 7(c)], the ratio is initially greater than unity but decreases below unity for large $N_{\max}$, and the changes in fact are becoming larger for successive $N_{\max}$. While there is a sharp downturn in the curves for $\hbar\omega \lesssim 10$, recall from Sec. III that the calculations for $\hbar\omega \lesssim 10\,\mathrm{MeV}$ for the Daejeon16 interactions may be of limited relevance to the physical ground state.

For $A = 9'$ [Figs. 6(f) and 7(d)], the spacing between successive $N_{\max}$ curves systematically decreases with increasing $N_{\max}$, hinting at eventual convergence, perhaps with a $\lesssim 10\%$ violation of mirror symmetry. This case is of special interest in the context of isospin symmetry, since these ^{9}Li and ^{9}C ground states bookend a $T = 3/2$ quartet of isobaric analog states noted for apparent violation of the isobaric multiplet mass equation [67, 68]. (The excited analog states in ^{9}Be and ^{9}B are above the single-nucleon separation threshold, and thus are subject to the Thomas-Ehrman effect [69, 70].)

For $A = 11$ [Figs. 6(g) and 7(e)], while the calculated $Q_p(^{11}\mathrm{C})/Q_n(^{11}\mathrm{B})$ changes comparatively little with $N_{\max}$, and the curves in Fig. 6(g) might superficially be taken to suggest an $\sim 3\%$ deviation from mirror symmetry, closer inspection shows that the calculated ratio still increases steadily with $N_{\max}$. There is thus no clear sign of convergence.

For the $A = 13$ pair [Figs. 6(i) and 7(g)], recall from Sec. III that the convergence behavior of $Q_p(^{13}\mathrm{O})$, and thus of the ratio, is anomalous [Fig. 4(i)], at least partly attributable to the semi-magic nature of these nuclei. It is therefore not obvious how to interpret the convergence behavior of the deviation from mirror symmetry.

Then, returning to the odd-odd nuclides, for $A = 8$ [Figs. 6(d) and 7(b)], the ratio continues to march upwards, with approximately constant spacing between calculations for successive $N_{\max}$. For $A = 12$ [Figs. 6(h) and 7(f)], the spacing is gradually decreasing, but the ultimate value to which this ratio will converge can only be estimated as likely giving a $< 10\%$ deviation from mirror symmetry.

It is interesting to compare these (unconverged) estimates of the deviation from mirror symmetry in the quadrupole moment with those found in the GFMC calculations [39]. In Ref. [39], both Q_p and Q_n were calculated independently for each member of the $A = 8$ and $9'$ mirror pairs (see note to Table I above), yielding $Q_p(^8\mathrm{B})/Q_n(^8\mathrm{Li}) = 0.91(7)$ and $Q_p(^9\mathrm{C})/Q_n(^9\mathrm{Li}) = 1.11(11)$. While both results are consistent with unity (or nearly so) within GFMC statistical uncertainties, intriguingly, the sense of the deviation differs from the present results for $A = 8$ [compare Fig. 7(b)] but agrees for $A = 9'$ [compare Fig. 7(d)]. The isospin violation in the wave functions provided by the GFMC calculations is severely restricted, as the GFMC propagator only takes the Coulomb interaction into account approximately (as an effective isoscalar Coulomb operator with a T_z-dependent normalization) and replaces the isospin-breaking AV18 interaction with the simpler isoscalar AV8′ interaction [71].

In summary, although the isospin quantum number in the *ab initio* NCCI calculations is quite "good", we should not be lulled by this observation into assuming the validity of mirror symmetry for observables in general, and for the quadrupole moments in particular. The traditional use of the mirror quadrupole moment as a proxy for Q_n must be treated with caution. The present calculations do not provide a firm estimate for the error thereby incurred: both since convergence is slow in the many-body calculation for the relevant observables (Fig. 6), but also potentially due to limitations in the isospin breaking contributions in the underlying interactions. Nonetheless, the calculations do suggest deviations of at least 5–10%, and potentially much larger.

V. INTERPRETATION OF THEORETICAL RESULTS

To extract information on the proton-neutron structure from calculations, of course, it is not necessary to use the mirror ratio (Sec. III) as a proxy for the ratio of neutron and proton quadrupole moments. This was simply imposed by experimental necessity. Rather, we may directly calculate Q_n/Q_p from the wave function for a given nuclide. Such results are shown for reference for the neutron rich member of each mirror pair in Fig. 8, from the present NCCI wave functions, alongside analogous results (for $A \leq 9$) from the GFMC calculations of Ref. [39]. Qualitatively there is little difference from the mirror ratio results shown in Fig. 5, to which these results are related by the mirror asymmetry ratios of Fig. 7 (which are admittedly unconverged, but remain numerically close to unity for the present calculations).

If qualitative understanding of the nuclear structure is sought, some further conceptual framework (or model) is needed to interpret these raw computed values. Here, after a few general initial comments, we simply note some possible fruitful avenues, involving clustering and dynam-

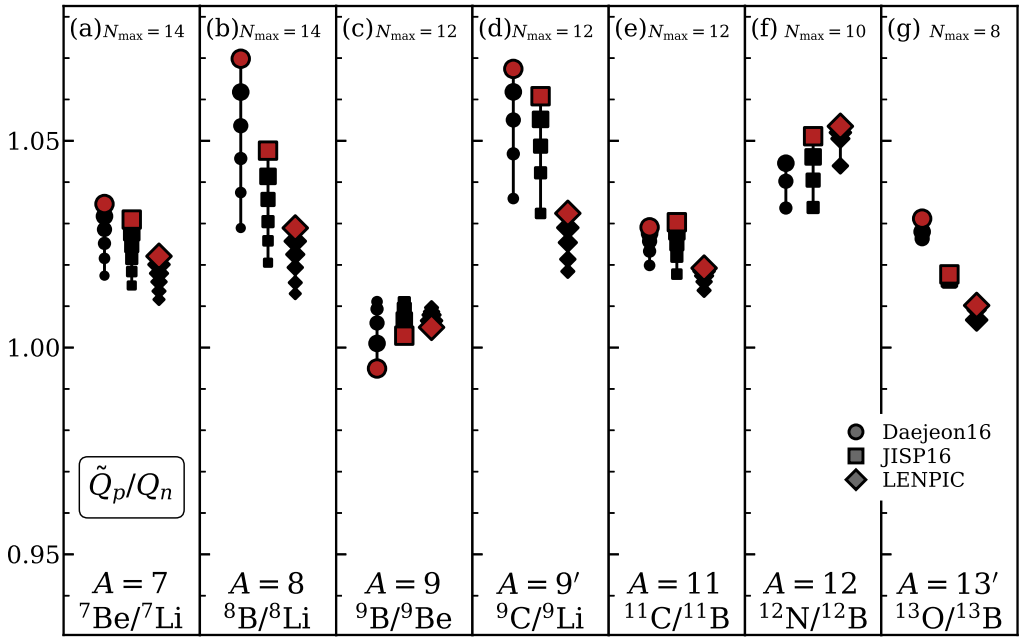

FIG. 7. Ratio of Q_p in one member of mirror pair to Q_n in the other, calculated with the Daejeon16 (circles), JISP16 (squares), and LENPIC (diamonds) interactions at fixed $\hbar\omega$ (15 MeV, 20 MeV, and 25 MeV, respectively, for the three interactions). Calculated values are shown for successive even values of N_{max} (increasing symbol size), from $N_{max} = 4$ to the maximum value for that mirror pair, indicated at top.

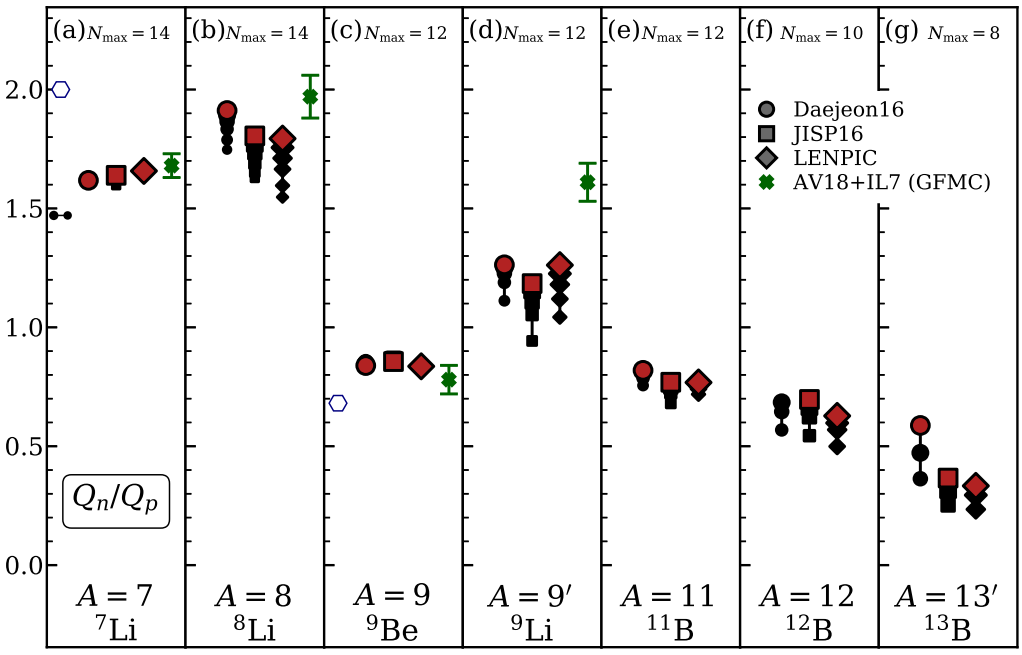

FIG. 8. Ratios Q_n/Q_p, for the neutron-rich members of the p-shell mirror pairs, calculated with the Daejeon16 (circles), JISP16 (squares), and LENPIC (diamonds) interactions at fixed $\hbar\omega$ (15 MeV, 20 MeV, and 25 MeV, respectively, for the three interactions). Calculated values are shown for successive even values of N_{max} (increasing symbol size), from $N_{max} = 4$ to the maximum value for that mirror pair, indicated at top. Also shown (see Table I) are the GFMC AV18+IL7 predictions [39] (crosses), along with a schematic cluster model estimate (see text) for ^{7}Li (dumbbell) and Elliott-Wilsdon SU(3) rotational model estimates for ^{7}Li and ^{9}Be (open hexagons).

ical symmetry.

A naive baseline estimate for Q_n/Q_p may be made in the spirit of the collective liquid drop interpretations of heavier nuclei, by taking the nucleus as a homogeneously charged matter distribution. In this case, the quadrupole operators for the protons and neutrons are identical except for overall normalization, proportional to Z/A for the protons [1] and N/A for the neutrons. We thus have $Q_n/Q_p = N/Z$, giving $Q_n/Q_p = 4/3 \approx 1.33$ for ^{7}Li, $Q_n/Q_p = 5/3 \approx 1.67$ for ^{8}Li, and so on, through $Q_n/Q_p = 8/5 \approx 1.6$ for ^{13}B. While these estimates are not egregiously far off from the calculations in Fig. 8 (or the experimental mirror ratios in Fig. 5), except in the ill-behaved case of $A = 13'$, neither do their variations from nuclide to nuclide particularly match or illuminate the trends in the ratios as one moves across Fig. 8.

The viewpoint that collectivity arises primarily in the valence shell might suggest rather that the numbers of *valence* nucleons of each species, *i.e.*, N_p for the protons and N_n for the neutrons [3], are more relevant than the total numbers, Z and N. However, this raises the thorny issue of the appropriate effective charges e_p and e_n to apply in an estimate $Q_n/Q_p = (e_n N_n)/(e_p N_p)$.

Indeed, the contrasting traditional model framework would be the shell model, and certainly valence shell calculations in the p shell can bear striking similarity to *ab initio* results [72] (see Fig. 13 of Ref. [19]). Detailed shell model studies [73] of the ground state quadrupole moments for several of the present nuclei, based on empirical isospin-nonconserving shell-model interactions [74], highlight the dependence of the calculated quadrupole moments in detail not only upon the effective charges but also upon the choice of shell model radial wave function (harmonic oscillator *vs.* Woods-Saxon).

Given the prominent role of clusterization in the structure of p-shell nuclides (*e.g.*, Refs. [31]), we may naturally seek to use *ab initio* calculated quadrupole moment ratios to test or provide constraints on interpretations based on clustering and the associated cluster molecular orbitals. In a clustering description, the naive assumption of a homogeneous charge distribution is manifestly broken, except in a few special cases (*e.g.*, pure α-cluster nuclei). For instance, in a cluster molecular orbital picture, the neutron-rich Be isotopes consist of a 2α dimer plus additional "valence" neutrons in molecular orbitals [31, 75–83]. A microscopic justification for this description is obtained from antisymmetrized molecular dynamics (AMD) [84–87], fermionic molecular dynamics (FMD) [88], or *ab initio* resonating group method (RGM) [89] calculations of the Be isotopes. The neutron quadrupole moment is sensitive to whether the neutrons occupy π ("equatorial") or σ ("polar") molecular orbitals, while the proton quadrupole moment is largely sensitive only to the inter-α separation.

Here it is interesting to note what we would expect from a schematic "ball and stick" molecular model for ^{7}Li. That is, suppose we take the ground state of ^{7}Li to have an $\alpha + t$ cluster structure, and then we reduce this description to the simple, naive limit of two point-like clusters, separated by a fixed, finite distance. The resulting structure would be an axially-symmetric rigid rotor. By the usual proportionality between laboratory-frame and intrinsic quadrupole moments for an axially-symmetric rotor [4], the ratio of the neutron and proton quadrupole moments in the laboratory frame would be identical to their ratio in the rotational intrinsic (principal axes) frame, that is, computed with respect to the molecular symmetry axis. This yields[2] an estimate of Q_n/Q_p just shy of 1.5, as indicated in Fig. 8(a) (dumbbell shape). Clearly, this picture ignores essential features of any more realistic cluster picture, such as the finite size of the clusters, which is comparable in scale to their separation, the consequent modification of the clusters by Fermi exclusion effects, as well as other polarization effects on the internal structure of the clusters, and zero-point oscillations in their separation. Yet the *ab initio* predictions, which are robustly consistent with each other in the range $Q_p/Q_n \approx 1.6$–1.7, provide a ratio only 10–15% larger than this schematic estimate.

At the other end of the mass range, recall the ill-behaved convergence of the proton quadrupole moment in ^{13}O [Fig. 4(i)]. This behavior, which now appears in the neutron quadrupole moment of ^{13}B, entering into the Q_n/Q_p ratio of Fig. 8(g), takes on new significance in a cluster molecular orbital interpretation, where ^{13}B is described as $2\alpha + 4n + p$. Here, it has been proposed [90] that the large ground state (proton) quadrupole moment reflects the result of mixing between two low-lying $3/2^-$ cluster configurations, obtained by coupling a proton in a π orbital (with $K = 3/2$) to the two low-lying 0^+ states of ^{12}Be. These ^{12}Be states, in turn, differ not only in inter-α separation, which affects the proton quadrupole moment, but also in whether the molecular orbitals occupied by the neutrons are π^4 (a low-deformation configuration) or $\pi^2\sigma^2$ (a high-deformation configuration) [81] (see also Fig. 5 of Ref. [87]), which may be expected to dramatically affect the neutron quadrupole moment.

Thus, in a clustering picture, the ground state Q_p and Q_n in ^{13}B reflect the shape coexistence in the low-lying spectrum of ^{12}Be (*e.g.*, Ref. [91]). Both moments, and Q_n in particular, should be sensitive to the resultant mixing of configurations with significantly different deformations. Meanwhile, in NCCI calculations, the relative energy for the ^{12}Be 0^+ states evolves rapidly with $N_{\max}$ (*e.g.*, Fig. 19 of Ref. [18]), ostensibly making any such mixing highly $N_{\max}$ dependent. Consistent with the proposed clustering picture of ^{13}B, the NCCI calculations also yield a predominantly $2\hbar\omega$ excited $3/2^-$ state, which

[2] The proton and neutron quadrupole moments must be calculated relative to the common center of mass, which lies 3/7 of the way from the alpha to the triton, putting the clusters at coordinates $z_\alpha = -3/7$ and $z_t = +4/7$, respectively, along the symmetry axis (in units of an arbitrary separation ℓ, which is irrelevant to the final ratio). Then, $Q_p = 2z_\alpha^2 + z_t^2$, and $Q_n = 2z_\alpha^2 + 2z_t^2$, giving $Q_n/Q_p = 50/34 \approx 1.47$.

converges rapidly downward in energy towards the predominantly $0\hbar\omega$ $3/2^-$ ground state, becoming the first excited state at high $N_{\max}$.

We may also seek to at least qualitatively understand the deviations from mirror symmetry (Sec. IV) in terms of cluster structure. In nuclei where prolate quadrupole deformation arises predominantly from the cluster dimer structure, the additional Coulomb repulsion obtained in going from the neutron-rich member of the mirror pair to the proton-rich member may be expected to increase the inter-cluster separation, and thus the quadrupole deformation. Thus, *e.g.*, in going from the neutrons in ^{7}Li to the protons in ^{7}Be [Fig. 7(a)], the increase in quadrupole moment Q_p for ^{7}Be relative to Q_n for ^{7}Li would be interpreted as arising from the increased repulsion and thus intercluster separation between the alpha and helion clusters in ^{7}Be ($= \alpha + h$) as compared to the alpha and triton clusters in ^{7}Li ($= \alpha + t$). (If variation in the internal structure of the clusters is also considered, then the extra Coulomb repulsion would also be expected to enhance the proton quadrupole moment by increasing the polarization of the clusters, such that the protons are further displaced towards the termini of the molecule.)

In contrast, if ^{9}Be and ^{9}B [Fig. 7(c)] are taken as $2\alpha+n$ and $2\alpha + p$, respectively, the valence nucleon is expected to be in an equatorial π orbital [31, 75, 78, 83] (see also Fig. 5 of Ref. [13] for *ab initio* predictions). This nucleon thus gives an oblate contribution to the deformation, serving to reduce the overall positive intrinsic quadrupole moment calculated with respect to the symmetry axis of the 2α dimer. An increase in the size of this orbital, induced by Coulomb repulsion, would therefore tend to reduce Q_p in ^{9}B relative to Q_n in ^{9}Be, an effect which would be in competition with any concomitant increase in the inter-α spacing in ^{9}B relative to ^{9}Be.

Symmetry-based descriptions provide an alternative route by which we may seek to understand the proton-neutron quadrupole structure revealed in *ab initio* calculations. The ground state wave functions of a variety of p-shell nuclides, in *ab initio* NCCI calculations, have been found to be remarkably well-described by a dominant contribution exhibiting Elliott SU(3) symmetry [92–98]. Elliott's SU(3) group [32, 33] has as its generators the components of a quadrupole tensor $\mathcal{Q}_2$ (this is Elliott's restricted quadrupole operator, which conserves oscillator quanta) and the orbital angular momentum vector L_1 (*e.g.*, Appendix A.4 of Ref. [44]). Elliott's SU(3) thus provides a symmetry-based description for the correlations which give rise to quadrupole deformation and rotation.

For the p-shell nuclides, Elliott's SU(3) model provides definite predictions for the quadrupole moment ratio Q_n/Q_p. In Elliot's SU(3) model, the ground state is expected to come from the "leading" SU(3) irreducible representation (irrep) in the $0\hbar\omega$ space. The states constituting this irrep are the most deformed in the $0\hbar\omega$ space, and thus most bound by Elliott's $-\mathcal{Q}\cdot\mathcal{Q}$ schematic Hamiltonian [33]. If we work in a proton-neutron SU(3) scheme, described by the group chain $\mathrm{SU}_p(3)\times\mathrm{SU}_n(3) \supset \mathrm{SU}(3)$, then the proton and neutron quadrupole operators are also generators. This permits simple analytic calculations for the proton and neutron quadrupole moments, to within an arbitrary overall scale (depending on the oscillator length of Sec. III A), which cancels in their ratio.

The ground-state SU(3) structure for ^{7}Li (or, equivalently, its mirror nuclide ^{7}Be) has been explored in *ab initio* calculations [22, 95, 97], showing that the $3/2^-$ ground state indeed comes predominantly from the leading irrep in the ^{7}Li $0\hbar\omega$ space, which has SU(3) quantum numbers $(\lambda,\mu) = (3,0)$ and total spin $S = 1/2$. The ground state in this description is uniquely defined, as a pure LS-coupling scheme state in which orbital angular momentum $L = 1$ combines with the spin to give $J = 3/2$ (see Fig. 1 of Ref. [97]). The resulting SU(3) estimate $Q_n/Q_p = 2$, shown in Fig. 7(a) (open hexagon), errs in the opposite direction from the naive cluster estimate above.

The expected ground state SU(3) structure for ^{9}Be has also been discussed extensively [22, 99, 100]. In the leading SU(3) irrep, which is $(3,1)$, with $S = 1/2$, a $J = 3/2$ state can be constructed two ways, by combining either $L = 1$ or $L = 2$ with the spin to give $J = 3/2$. The physical ground state may be expected to be some mixture of these. Although the $L = 1$ state has lower rotational energy, in the Elliott-Wilsdon rotational model [32, 33] the spin-orbit interaction mixes these states to give a $K = 3/2$ rotational bandhead state $|K = 3/2; J = 3/2\rangle = \sqrt{21/26}|L = 1; J = 3/2\rangle - \sqrt{5/26}|L = 2; J = 3/2\rangle$ [99]. The resulting SU(3) estimate $Q_n/Q_p \approx 0.68$ [Fig. 7(c)] lies only marginally below the *ab initio* predictions.

VI. CONCLUSION

In summary, meaningful predictions of electric quadrupole moment ratios can be made, in *ab initio* NCCI calculations, even though the moments themselves are not individually converged. This observation applies more generally to ratios of electromagnetic matrix elements involving states with similar convergence properties, arising from structural similarities. Examples include (ratios of) transition strengths within a rotational band [18, 22], or between rotational bands with related structures [25], or across mirror transitions [26].

In particular, ratios of electric quadrupole moments in mirror nuclei provide an observable which can be both, on one hand, precisely measured experimentally and, on the other hand, well-converged in NCCI calculations, thereby providing stringent tests of the theoretical framework. Where the experimental ratio is known, and where a robust prediction can be meaningfully extracted from the NCCI calculations, we find generally good agreement (Fig. 5). Alternatively, where the moment of only one member of the mirror pair is known, NCCI calculations

can be taken to provide predictive power for the other unknown moment.

However, it must be emphasized that precision *ab initio* predictions of electric quadrupole moment ratios are not always possible. A robust prediction for the ratio may be understood as arising when the incomplete convergence of the quadrupole moments themselves is simply a systematic effect of the basis truncation, to be cancelled out between the moments, but not if the moments are exquisitely sensitive to fine details of the many-body calculation, *e.g.*, delicate mixing of competing low-lying configurations.

By isospin mirror symmetry, the ratio of electric quadrupole moments across mirror nuclei is closely related, though not strictly equivalent (Fig. 7), to the neutron/proton quadrupole moment ratio within a single nuclide. Although the neutron quadrupole moment itself is not directly accessible experimentally, *ab initio* calculations can provide robust predictions for the neutron/proton quadrupole moment ratio (Fig. 8), thereby giving insight into the isovector aspects of the quadrupole deformation. In the limit of axially-symmetric adiabatic rotation, this ratio measures the relative contributions of the neutrons and protons to the deformation. More generally, it is subject to interpretation through effective descriptions of the proton-neutron structure of the nucleus, *e.g.*, involving simpler degrees of freedom, as in clustering, or correlations imposed by symmetry, as in the Elliott SU(3) picture.

ACKNOWLEDGMENTS

We thank Saori Pastore and James P. Vary for valuable discussions and Jingru Z. Benner, Colin V. Coane, Jakub Herko, and Zhou Zhou for comments on the paper. This material is based upon work supported by the U.S. Department of Energy, Office of Science, under Award Numbers DE-FG02-95ER40934, DE-FG02-00ER41132, and DESC00018223 (SciDAC4/NUCLEI). An award of computer time was provided by the Innovative and Novel Computational Impact on Theory and Experiment (INCITE) program. This research used computational resources of the National Energy Research Scientific Computing Center (NERSC) and the Argonne Leadership Computing Facility (ALCF), which are U.S. Department of Energy, Office of Science, user facilities, supported under Contract Numbers DE-AC02-05CH11231 and DE-AC02-06CH11357.

[1] J. M. Eisenberg and W. Greiner, *Nuclear Theory*, 3rd ed., Vol. 1 (North-Holland, Amsterdam, 1987).
[2] A. Bohr and B. R. Mottelson, *Nuclear Structure*, Vol. 2 (World Scientific, Singapore, 1998).
[3] R. F. Casten, *Nuclear Structure from a Simple Perspective*, 2nd ed., Oxford Studies in Nuclear Physics No. 23 (Oxford University Press, Oxford, 2000).
[4] D. J. Rowe, *Nuclear Collective Motion: Models and Theory* (World Scientific, Singapore, 2010).
[5] D. J. Rowe and J. L. Wood, *Fundamentals of Nuclear Models: Foundational Models* (World Scientific, Singapore, 2010).
[6] T. Minamisono, T. Ohtsubo, I. Minami, S. Fukuda, A. Kitagawa, M. Fukuda, K. Matsuta, Y. Nojiri, S. Takeda, H. Sagawa, and H. Kitagawa, Proton halo of ^{8}B disclosed by its giant quadrupole moment, Phys. Rev. Lett. **69**, 2058 (1992).
[7] H. Kitagawa and H. Sagawa, Quadrupole-moments in mirror nuclei and proton halo, Phys. Lett. B **299**, 1 (1993).
[8] N. J. Stone, Table of nuclear electric quadrupole moments, At. Data Nucl. Data Tables **111**, 1 (2016).
[9] A. Bernstein, V. Brown, and V. Madsen, Neutron and proton transition matrix elements and inelastic hadron scattering, Phys. Lett. B **103**, 255 (1981); Neutron and proton matrix elements for low-lying 2^+ transitions and the probe dependence of the nuclear deformation parameter, Comments Nucl. Part. Phys. **11**, 203 (1983).
[10] E. M. Henley, Charge independence and charge symmetry of nuclear forces, in *Isospin in Nuclear Physics*, edited by D. H. Wilkinson (North-Holland, Amsterdam, 1969) p. 15.
[11] S. C. Pieper, R. B. Wiringa, and J. Carlson, Quantum Monte Carlo calculations of excited states in $A = 6$–8 nuclei, Phys. Rev. C **70**, 054325 (2004).
[12] T. Neff and H. Feldmeier, Cluster structures within fermionic molecular dynamics, Nucl. Phys. A **738**, 357 (2004).
[13] P. Maris, *Ab initio* nuclear structure calculations of light nuclei, J. Phys. Conf. Ser. **402**, 012031 (2012).
[14] T. Yoshida, N. Shimizu, T. Abe, and T. Otsuka, Intrinsic structure of light nuclei in Monte Carlo shell model calculation, Few-Body Syst. **54**, 1465 (2013).
[15] C. Romero-Redondo, S. Quaglioni, P. Navrátil, and G. Hupin, How many-body correlations and α clustering shape ^{6}He, Phys. Rev. Lett. **117**, 222501 (2016).
[16] P. Navrátil, S. Quaglioni, G. Hupin, C. Romero-Redondo, and A. Calci, Unified *ab initio* approaches to nuclear structure, Physica Scripta **91**, 053002 (2016).
[17] M. A. Caprio, P. Maris, and J. P. Vary, Emergence of rotational bands in *ab initio* no-core configuration interaction calculations of light nuclei, Phys. Lett. B **719**, 179 (2013).
[18] P. Maris, M. A. Caprio, and J. P. Vary, Emergence of rotational bands in *ab initio* no-core configuration interaction calculations of the Be isotopes, Phys. Rev. C **91**, 014310 (2015); Erratum: Emergence of rotational bands in *ab initio* no-core configuration interaction calculations of the Be isotopes, Phys. Rev. C **99**, 029902(E) (2019).
[19] M. A. Caprio, P. Maris, J. P. Vary, and R. Smith, Collective rotation from *ab initio* theory, Int. J. Mod. Phys. E **24**, 1541002 (2015).
[20] S. R. Stroberg, H. Hergert, J. D. Holt, S. K. Bogner, and

A. Schwenk, Ground and excited states of doubly open-shell nuclei from *ab initio* valence-space hamiltonians, Phys. Rev. C **93**, 051301 (2016).
[21] G. R. Jansen, M. D. Schuster, A. Signoracci, G. Hagen, and P. Navrátil, Open *sd*-shell nuclei from first principles, Phys. Rev. C **94**, 011301 (2016).
[22] M. A. Caprio, P. J. Fasano, P. Maris, A. E. McCoy, and J. P. Vary, Probing *ab initio* emergence of nuclear rotation, Eur. Phys. J. A **56**, 120 (2020).
[23] B. R. Barrett, P. Navrátil, and J. P. Vary, *Ab initio* no core shell model, Prog. Part. Nucl. Phys. **69**, 131 (2013).
[24] P. Maris and J. P. Vary, *Ab initio* nuclear structure calculations of *p*-shell nuclei with JISP16, Int. J. Mod. Phys. E **22**, 1330016 (2013).
[25] M. A. Caprio, P. J. Fasano, A. E. McCoy, P. Maris, and J. P. Vary, *Ab initio* rotation in ^{10}Be, Bulg. J. Phys. **46**, 445 (2019).
[26] S. L. Henderson, T. Ahn, M. A. Caprio, P. J. Fasano, A. Simon, W. Tan, P. O'Malley, J. Allen, D. W. Bardayan, D. Blankstein, B. Frentz, M. R. Hall, J. J. Kolata, A. E. McCoy, S. Moylan, C. S. Reingold, S. Y. Strauss, and R. O. Torres-Isea, First measurement of the $B(E2; 3/2^- \to 1/2^-)$ transition strength in ^{7}Be: Testing *ab initio* predictions for $A = 7$ nuclei, Phys. Rev. C **99**, 064320 (2019).
[27] A. M. Shirokov, I. J. Shin, Y. Kim, M. Sosonkina, P. Maris, and J. P. Vary, N3LO NN interaction adjusted to light nuclei in *ab exitu* approach, Phys. Lett. B **761**, 87 (2016).
[28] A. M. Shirokov, J. P. Vary, A. I. Mazur, and T. A. Weber, Realistic nuclear Hamiltonian: *Ab exitu* approach, Phys. Lett. B **644**, 33 (2007).
[29] E. Epelbaum, H. Krebs, and U.-G. Meißner, Precision nucleon-nucleon potential at fifth order in the chiral expansion, Phys. Rev. Lett. **115**, 122301 (2015).
[30] E. Epelbaum, H. Krebs, and U.-G. Meißner, Improved chiral nucleon-nucleon potential up to next-to-next-to-next-to-leading order, Eur. Phys. J. A **51**, 53 (2015).
[31] M. Freer, The clustered nucleus—cluster structures in stable and unstable nuclei, Rep. Prog. Phys. **70**, 2149 (2007).
[32] J. P. Elliott, Collective motion in the nuclear shell model. I. Classification schemes for states of mixed configurations, Proc. R. Soc. London A **245**, 128 (1958); Collective motion in the nuclear shell model. II. The introduction of intrinsic wave functions, Proc. R. Soc. London A **245**, 562 (1958); J. P. Elliott and M. Harvey, Collective motion in the nuclear shell model. III. The calculation of spectra, Proc. R. Soc. London A **272**, 557 (1963); J. P. Elliott and C. E. Wilsdon, Collective motion in the nuclear shell model. IV. Odd-mass nuclei in the *sd* shell, Proc. R. Soc. London A **302**, 509 (1968).
[33] M. Harvey, The nuclear SU_3 model, in *Advances in Nuclear Theory*, Vol. 1, edited by M. Baranger and E. Vogt (Plenum, New York, 1968) p. 67.
[34] D. R. Tilley, C. M. Cheves, J. L. Godwin, G. M. Hale, H. M. Hofmann, J. H. Kelley, C. G. Sheu, and H. R. Weller, Energy levels of light nuclei $A = 5, 6, 7$, Nucl. Phys. A **708**, 3 (2002).
[35] D. R. Tilley, J. H. Kelley, J. L. Godwin, D. J. Millener, J. E. Purcell, C. G. Sheu, and H. R. Weller, Energy levels of light nuclei $A = 8$, 9, 10, Nucl. Phys. A **745**, 155 (2004).
[36] F. Ajzenberg-Selove, Energy levels of light nuclei $A =$ 11–12, Nucl. Phys. A **506**, 1 (1990).
[37] F. Ajzenberg-Selove, Energy levels of light nuclei $A =$ 13–15, Nucl. Phys. A **523**, 1 (1991).
[38] J. Kelley, E. Kwan, J. E. Purcell, C. G. Sheu, and H. R. Weller, Energy levels of light nuclei $A = 11$, Nucl. Phys. A **880**, 88 (2012).
[39] S. Pastore, S. C. Pieper, R. Schiavilla, and R. B. Wiringa, Quantum Monte Carlo calculations of electromagnetic moments and transitions in $A \leq 9$ nuclei with meson-exchange currents derived from chiral effective field theory, Phys. Rev. C **87**, 035503 (2013).
[40] T. Minamisono, T. Ohtsubo, K. Sato, S. Takeda, S. Fukuda, T. Izumikawa, M. Tanigaki, T. Miyake, T. Yamaguchi, N. Nakamura, H. Tanji, K. Matsuta, M. Fukuda, and Y. Nojiri, Quadrupole moment of the proton rich β-emitting nucleus ^{12}N, Phys. Lett. B **420**, 31 (1998).
[41] A. Schirmacher and H. Winter, High-resolution quantum-beat and rf resonance spectroscopy after grazing-ion–surface scattering and its application in studies of the hyperfine structure of stable terms in ^{14}N I, II, and III, Phys. Rev. A **47**, 4891 (1993).
[42] N. J. Stone, Table of nuclear magnetic dipole and electric quadrupole moments, At. Data Nucl. Data Tables **90**, 75 (2005).
[43] P. Pyykkö, Year-2008 nuclear quadrupole moments, Mol. Phys. **106**, 1965 (2008).
[44] M. A. Caprio, A. E. McCoy, and P. J. Fasano, Intrinsic operators for the translationally-invariant many-body problem, J. Phys. G **47**, 122001 (2020).
[45] J. Suhonen, *From Nucleons to Nucleus* (Springer-Verlag, Berlin, 2007).
[46] H. M. Aktulga, C. Yang, E. G. Ng, P. Maris, and J. P. Vary, Improving the scalability of symmetric iterative eigensolver for multi-core platforms, Concurrency Computat.: Pract. Exper. **26**, 2631 (2013).
[47] M. Shao, H. M. Aktulga, C. Yang, E. G. Ng, P. Maris, and J. P. Vary, Accelerating nuclear configuration interaction calculations through a preconditioned block iterative eigensolver, Comput. Phys. Commun. **222**, 1 (2018).
[48] A. Nogga, P. Navrátil, B. R. Barrett, and J. P. Vary, Spectra and binding energy predictions of chiral interactions for ^{7}Li, Phys. Rev. C **73**, 064002 (2006).
[49] S. K. Bogner, R. J. Furnstahl, P. Maris, R. J. Perry, A. Schwenk, and J. Vary, Convergence in the no-core shell model with low-momentum two-nucleon interactions, Nucl. Phys. A **801**, 21 (2008).
[50] C. Cockrell, J. P. Vary, and P. Maris, Lithium isotopes within the *ab initio* no-core full configuration approach, Phys. Rev. C **86**, 034325 (2012).
[51] M. A. Caprio, P. Maris, and J. P. Vary, Halo nuclei ^{6}He and ^{8}He with the Coulomb-Sturmian basis, Phys. Rev. C **90**, 034305 (2014).
[52] D. Odell, T. Papenbrock, and L. Platter, Infrared extrapolations of quadrupole moments and transitions, Phys. Rev. C **93**, 044331 (2016).
[53] D. R. Entem and R. Machleidt, Accurate charge-dependent nucleon-nucleon potential at fourth order of chiral perturbation theory, Phys. Rev. C **68**, 041001 (2003).
[54] S. K. Bogner, R. J. Furnstahl, and R. J. Perry, Similarity renormalization group for nucleon-nucleon interactions, Phys. Rev. C **75**, 061001 (2007).

[55] P. Maris, I. J. Shin, and J. P. Vary, *Ab initio* structure of p-shell nuclei with chiral effective field theory and Daejeon16 interactions, in *Proceedings of the International Conference Nuclear Theory in the Supercomputing Era 2018*, edited by A. M. Shirokov and A. I. Mazur (Pacific National University, Khabarovsk, Russia, 2019) p. 168.

[56] S. Binder, A. Calci, E. Epelbaum, R. J. Furnstahl, J. Golak, K. Hebeler, H. Kamada, H. Krebs, J. Langhammer, S. Liebig, P. Maris, U.-G. Meißner, D. Minossi, A. Nogga, H. Potter, R. Roth, R. Skibiński, K. Topolnicki, J. P. Vary, and H. Witała, Few-nucleon systems with state-of-the-art chiral nucleon-nucleon forces, Phys. Rev. C **93**, 044002 (2016).

[57] S. Binder, A. Calci, E. Epelbaum, R. J. Furnstahl, J. Golak, K. Hebeler, T. Hüther, H. Kamada, H. Krebs, P. Maris, U.-G. Meißner, A. Nogga, R. Roth, R. Skibiński, K. Topolnicki, J. P. Vary, K. Vobig, and H. Witała (LENPIC Collaboration), Few-nucleon and many-nucleon systems with semilocal coordinate-space regularized chiral nucleon-nucleon forces, Phys. Rev. C **98**, 014002 (2018).

[58] See Supplemental Material at http://xxxxxxxx for tabulations of the calculated quadrupole moments, as functions of $N_{\max}$ and $\hbar\omega$.

[59] J. Carlson, S. Gandolfi, F. Pederiva, S. C. Pieper, R. Schiavilla, K. E. Schmidt, and R. B. Wiringa, Quantum Monte Carlo methods for nuclear physics, Rev. Mod. Phys. **87**, 1067 (2015).

[60] R. B. Wiringa, V. G. J. Stoks, and R. Schiavilla, Accurate nucleon-nucleon potential with charge-independence breaking, Phys. Rev. C **51**, 38 (1995).

[61] S. C. Pieper, The Illinois extension to the Fujita-Miyazawa three-nucleon force, in *New Facet of Three Nucleon Force — 50 Years of Fujita Miyazawa Three Nucleon Force (FM50): Proceedings of the International Symposium on New Facet of Three Nucleon Force*, AIP Conf. Proc. No. 1011, edited by H. Sakai, K. Sekiguchi, and B. F. Gibson (AIP, New York, 2008) pp. 143–152.

[62] K. R. Henninger, T. Neff, and H. Feldmeier, ^{8}B structure in fermionic molecular dynamics, J. Phys. Conf. Ser. **599**, 012038 (2015).

[63] S. L. Henderson, T. Ahn, M. A. Caprio, P. J. Fasano, A. E. McCoy, S. Aguilar, D. T. Blankstein, L. Caves, A. Dombos, R. K. Grzywacz, K. L. Jones, S. Jin, R. Kelmar, J. J. Kolata, P. D. O'Malley, C. S. Reingold, A. Simon, and K. Smith, Remeasuring the anomalously enhanced $B(E2; 2^+ \to 1^+)$ in ^{8}Li and comparison to *ab initio* predictions, Phys. Rev. C (submitted), arXiv:2109.06081 [nucl-ex].

[64] E. Epelbaum, H.-W. Hammer, and U.-G. Meißner, Modern theory of nuclear forces, Rev. Mod. Phys. **81**, 1773 (2009).

[65] G. P. Kamuntavičius, P. Navrátil, B. R. Barrett, G. Sapragonaite, and R. K. Kalinauskas, Isoscalar Hamiltonians for light atomic nuclei, Phys. Rev. C **60**, 044304 (1999).

[66] V. G. Gueorguiev, P. Navrátil, J. P. Vary, J. P. Draayer, and F. Pan, Challenges for modeling nuclear structure: Are the proton and neutron masses and A-body interactions relevant?, in *Nuclear Theory*, Vol. 29, edited by A. Georgieva and N. Minkov (Heron Press, Sofia, 2010) p. 228.

[67] M. Brodeur, T. Brunner, S. Ettenauer, A. Lapierre, R. Ringle, B. A. Brown, D. Lunney, and J. Dilling, Elucidation of the anomalous $A = 9$ isospin quartet behavior, Phys. Rev. Lett. **108**, 212501 (2012).

[68] Y. H. Lam, B. Blank, N. A. Smirnova, J. B. Bueb, and M. S. Antony, The isobaric multiplet mass equation for $A \leq 71$ revisited, At. Data Nucl. Data Tables **99**, 680 (2013).

[69] J. B. Ehrman, On the displacement of corresponding energy levels of C^{13} and N^{13}, Phys. Rev. **81**, 412 (1951).

[70] R. G. Thomas, An analysis of the energy levels of the mirror nuclei, C^{13} and N^{13}, Phys. Rev. **88**, 1109 (1952).

[71] B. S. Pudliner, V. R. Pandharipande, J. Carlson, S. C. Pieper, and R. B. Wiringa, Quantum Monte Carlo calculations of nuclei with $A < 7$, Phys. Rev. C **56**, 1720 (1997).

[72] C. W. Johnson, Spin-orbit decomposition of *ab initio* nuclear wave functions, Phys. Rev. C **91**, 034313 (2015).

[73] N. A. Smirnova and C. Volpe, On the asymmetry of Gamow–Teller β-decay rates in mirror nuclei in relation with second-class currents, Nucl. Phys. A **714**, 441 (2003).

[74] W. E. Ormand and B. A. Brown, Empirical isospin-nonconserving Hamiltonians for shell-model calculations, Nucl. Phys. A **491**, 1 (1989).

[75] J. Hiura and I. Shimodaya, Alpha-particle model for Be^9, Prog. Theor. Phys. **30**, 585 (1963); Errata: Alpha-particle model for Be^9, Prog. Theor. Phys. **31**, 165 (1964).

[76] S. Okabe, Y. Abe, and H. Tanaka, The structure of ^{9}Be nucleus by a molecular model. I, Prog. Theor. Phys. **57**, 866 (1979); S. Okabe and Y. Abe, The structure of ^{9}Be nucleus by a molecular model. II, Prog. Theor. Phys. **61**, 1049 (1979).

[77] M. Seya, M. Kohno, and S. Nagata, Nuclear binding mechanism and structure of neutron-rich Be and B isotopes by molecular-orbital model, Prog. Theor. Phys. **65**, 204 (1981).

[78] W. von Oertzen, Two-center molecular states in ^{9}B, ^{9}Be, ^{10}Be, and ^{10}B, Z. Phys. A **354**, 37 (1996).

[79] W. von Oertzen, Dimers based on the $\alpha + \alpha$ potential and chain states of carbon isotopes, Z. Phys. A **357**, 355 (1997).

[80] N. Itagaki and S. Okabe, Molecular orbital structures in ^{10}Be, Phys. Rev. C **61**, 044306 (2000).

[81] N. Itagaki, S. Okabe, and K. Ikeda, Important role of the spin-orbit interaction in forming the $1/2^+$ orbital structure in Be isotopes, Phys. Rev. C **62**, 034301 (2000).

[82] V. Della Rocca, R. Bijker, and F. Iachello, Single-particle levels in cluster potentials, Nucl. Phys. A **966**, 158 (2017).

[83] V. Della Rocca and F. Iachello, Cluster shell model: I. structure of ^{9}Be, ^{9}B, Nucl. Phys. A **973**, 1 (2018).

[84] Y. Kanada-En'yo and H. Horiuchi, Opposite deformations between protons and neutrons in proton-rich C isotopes, Phys. Rev. C **55**, 2860 (1997).

[85] Y. Kanada-En'yo, H. Horiuchi, and A. Doté, Structure of excited states of ^{10}Be studied with antisymmetrized molecular dynamics, Phys. Rev. C **60**, 064304 (1999).

[86] T. Suhara and Y. Kanada-En'yo, Quadrupole deformation β and γ constraint in a framework of antisymmetrized molecular dynamics, Prog. Theor. Phys. **123**, 303 (2010).

[87] Y. Kanada-En'yo, M. Kimura, and A. Ono, Antisymmetrized molecular dynamics and its applications to cluster phenomena, Prog. Exp. Theor. Phys. **2012**,

01A202 (2012).
[88] M. Žáková, Z. Andjelkovic, M. L. Bissell, K. Blaum, G. W. F. Drake, C. Geppert, M. Kowalska, J. Krämer, A. Krieger, M. Lochmann, T. Neff, R. Neugart, W. Nörtershäuser, R. Sánchez, F. Schmidt-Kaler, D. Tiedemann, Z.-C. Yan, D. T. Yordanov, and C. Zimmermann, Isotope shift measurements in the $2s_{1/2} \rightarrow 2p_{3/2}$ transition of Be^+ and extraction of the nuclear charge radii for ^{7,10,11}Be, J. Phys. G **37**, 055107 (2010).
[89] K. Kravvaris and A. Volya, Study of nuclear clustering from an *ab initio* perspective, Phys. Rev. Lett. **119**, 062501 (2017).
[90] S. Okabe, as discussed in Ref. [77].
[91] S. Shimoura, S. Ota, K. Demichi, N. Aoi, H. Baba, Z. Elekes, T. Fukuchi, T. Gomi, K. Hasegawa, E. Ideguchi, M. Ishihara, N. Iwasa, H. Iwasaki, S. Kanno, S. Kubono, K. Kurita, M. Kurokawa, Y. Matsuyama, S. Michimasa, K. Miller, T. Minemura, T. Motobayashi, T. Murakami, M. Notani, A. Odahara, A. Saito, H. Sakurai, E. Takeshita, S. Takeuchi, M. Tamaki, T. Teranishi, K. Yamada, Y. Yanagisawa, and I. Hamamoto, Lifetime of the isomeric 0_2^+ state in ^{12}Be, Phys. Lett. B **654**, 87 (2007).
[92] T. Dytrych, K. D. Launey, J. P. Draayer, P. Maris, J. P. Vary, E. Saule, U. Catalyurek, M. Sosonkina, D. Langr, and M. A. Caprio, Collective modes in light nuclei from first principles, Phys. Rev. Lett. **111**, 252501 (2013).
[93] K. D. Launey, T. Dytrych, and J. P. Draayer, Symmetry-guided large-scale shell-model theory, Prog. Part. Nucl. Phys. **89**, 101 (2016).
[94] K. Kravvaris and A. Volya, Study of clustering in isotopes of beryllium, in *Proceedings of the 4th International Workshop on "State of the Art in Nuclear Cluster Physics" (SOTANCP4)*, AIP Conf. Proc. No. 2038, edited by M. Barbui, C. M. Folden, III, V. Z. Goldberg, and G. V. Rogachev (AIP, New York, 2018) p. 020026.
[95] A. E. McCoy, *Ab initio multi-irrep symplectic no-core configuration interaction calculations*, Ph.D. thesis, University of Notre Dame (2018).
[96] A. E. McCoy, M. A. Caprio, and T. Dytrych, Symplectic no-core configuration interaction framework for *ab initio* nuclear structure, Ann. Acad. Rom. Sci. Ser. Phys. Chem. Sci. **3**, 17 (2018).
[97] A. E. McCoy, M. A. Caprio, T. Dytrych, and P. J. Fasano, Emergent $Sp(3,\mathbb{R})$ dynamical symmetry in the nuclear many-body system from an *ab initio* description, Phys. Rev. Lett. **125**, 102505 (2020).
[98] R. Zbikowski, C. W. Johnson, A. E. McCoy, M. A. Caprio, and P. J. Fasano, Rotational bands beyond the Elliott model, J. Phys. G **48**, 075102 (2021).
[99] D. J. Millener, Structure of unstable light nuclei, Nucl. Phys. A **693**, 394 (2001).
[100] D. J. Millener, Hypernuclear gamma-ray spectroscopy and the structure of p-shell nuclei and hypernuclei, in *Topics in Strangeness Nuclear Physics*, Lecture Notes in Physics, Vol. 724, edited by P. Bydžovský, J. Mareš, and A. Gal (Springer, Berlin, 2007) pp. 31–79.